AD-A094 249 ARIZONA UNIV TUCSON ENGINEERING EXPERIMENT STATION F/G 20/13
CONVECTIVE HEAT TRANSFER FOR SHIP PROPULSION.(U)
JAN 80 S E FAAS, D M MCELIGOT N00014-75-C-0694
UNCLASSIFIED 1248-7 NL

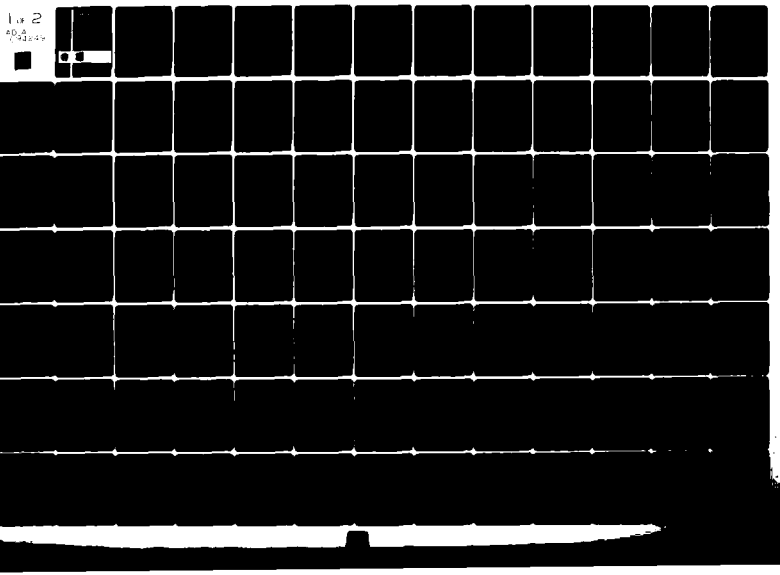

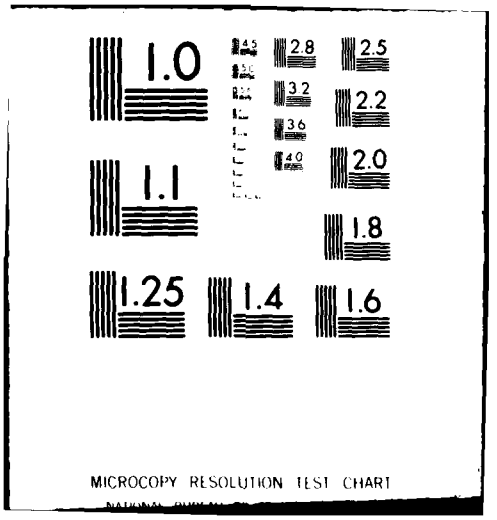
1.0
1.1
1.25
1.4
1.6
1.8
2.0
2.2
2.5
2.8
3.2
3.6
4.0
MICROCOPY RESOLUTION TEST CHART

LEVEL II

Fifth Annual Summary Report

Contract No. N00014-75-C-0694
Contract Authority NR-097-395

CONVECTIVE HEAT TRANSFER FOR SHIP PROPULSION

Prepared for

Office of Naval Research
Code 473
Arlington, Virginia

Prepared by

S. E. Faas and D. M. McEligot

15 January 1980

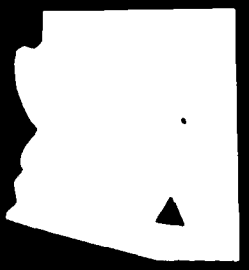

ENGINEERING EXPERIMENT STATION
COLLEGE OF ENGINEERING
THE UNIVERSITY OF ARIZONA
TUCSON, ARIZONA

Unclassified

SECURITY CLASSIFICATION OF THIS PAGE (When Data Entered)

REPORT DOCUMENTATION PAGE	READ INSTRUCTIONS BEFORE COMPLETING FORM
1. REPORT NUMBER: 1248-7 ✓	2. GOVT ACCESSION NO.: AD-A094 149
3. RECIPIENT'S CATALOG NUMBER:	
4. TITLE (and Subtitle): Convective Heat Transfer for Ship Propulsion. ~~(Fifth Annual Summary Report)~~	5. TYPE OF REPORT & PERIOD COVERED: Annual Summary Report, 1 April 1978 — 14 Jan. 1980
	6. PERFORMING ORG. REPORT NUMBER:
7. AUTHOR(s): Scott E. Faas ~~and~~ D. M. McEligot	8. CONTRACT OR GRANT NUMBER(s): N00014-75-C-0694 ✓
9. PERFORMING ORGANIZATION NAME AND ADDRESS: Engineering Experiment Station ✓ University of Arizona Tucson, Arizona 85721	10. PROGRAM ELEMENT, PROJECT, TASK AREA & WORK UNIT NUMBERS: NR-097-395
11. CONTROLLING OFFICE NAME AND ADDRESS: Office of Naval Research Code 473 Arlington, Virginia 22217	12. REPORT DATE: 30 Jan. 1980
	13. NUMBER OF PAGES: 86
14. MONITORING AGENCY NAME & ADDRESS (if different from Controlling Office): Office of Naval Research Bandolier Hall West - Rm. 204 University of New Mexico Albuquerque, N. M. 87131	15. SECURITY CLASS. (of this report): Unclassified
	15a. DECLASSIFICATION/ DOWNGRADING SCHEDULE

16. DISTRIBUTION STATEMENT (of this Report)

Unlimited

DISTRIBUTION STATEMENT A
Approved for public release;
Distribution Unlimited

17. DISTRIBUTION STATEMENT (of the abstract entered in Block 20, if different from Report)

Unlimited

DTIC ELECTE JAN 23 1981 S

18. SUPPLEMENTARY NOTES

19. KEY WORDS (Continue on reverse side if necessary and identify by block number)

Heat transfer
Laminar flow
Forced convection
Rough surfaces
Elliptic partial differential equations
Spacewise periodic flow
Fracture flow
Crack flow
Heat exchangers
Ducts

20. ABSTRACT (Continue on reverse side if necessary and identify by block number)

As duct configurations of interest in heat exchanger designs and other components in propulsion systems, a corrugated duct and a parallel plate duct with repeated rib roughness were selected for numerical modeling. For the rough duct, the flow field and the temperature distribution in both the fluid and in the solid plate were obtained. Results for the corrugated duct reveal the presence of large recirculating zones at Reynolds numbers greater than about 50. The friction factor passes through a minimum as the Reynolds number is increased and then approaches an approximately constant value corresponding to the development of the recirculation zones.

DD FORM 1 JAN 73 1473

Unclassified

SECURITY CLASSIFICATION OF THIS PAGE (When Data Entered)

Fifth Annual Summary Report

CONVECTIVE HEAT TRANSFER FOR SHIP PROPULSION

By

S. E. Faas and D. M. McEligot
Aerospace and Mechanical Engineering Department
University of Arizona
Tucson, Arizona 85721

Research Sponsored by

Office of Naval Research
ONR Contract Number N00014-75-C-0694
ONR Contract Authority NR-097-395

15 January 1980

ABSTRACT

Established, steady-state flow beyond the entry region in a duct with periodic wall geometry is hypothesized as spatially periodic. Spatially periodic flow is considered to be attained when the flow and heat transfer in any cycle of periodic wall geometry is identical to the cycle before and after it. Thus, a two-dimensional duct with periodic wall geometry may have its established flow far from the entrance predicted by a numerical solution over a cycle of the geometry.

A corrugated duct and a parallel plate duct with repeated rib roughness were selected for numerical modeling. These duct configurations are of interest in heat exchanger designs and other components in propulsion systems.

A numerical method, utilizing the general finite-difference program TEACH from Imperial College, was successfully developed to solve for fully established, laminar flow in a corrugated duct. This method was subsequently applied to predict laminar flow and heat transfer downstream in a parallel plate duct with repeated ribs as surface roughness elements.

Results for the corrugated duct reveal the presence of large recirculation zones at Reynolds numbers greater than about 50. The average friction factor varies inversely with the Reynolds number at low flow rates. It then passes through a minimum, as the Reynolds number is varied, and increases, apparently approaching an approximately constant value corresponding to the development of the recirculation zones.

Results for the rough duct are preliminary, but indicate reasonable results may be obtained. Both the flow field and the temperature distribution in the solid plate are determined, thereby providing means to predict the heat transfer behavior when the thermal resistance in the fluid and the thermal resistance in the wall are of the same order of magnitude.

TABLE OF CONTENTS

TABLE OF CONTENTS--Continued

LIST OF TABLES

LIST OF ILLUSTRATIONS

LIST OF ILLUSTRATIONS--Continued

NOMENCLATURE

Symbol	Definition
a	Distance between corner regions, m
D_h	Hydraulic diameter, m
f	Friction factor
g	Corrugated channel gap, m
H	Maximum width of corrugated channel, m
h	Rib height, m
k	Thermal conductivity, W/m-°C
ℓ	Contour co-ordinate, m
L_m	Mean distance between corresponding planes, m
$\dot{m}$	Mass Flow Rate, kg/s
N_n	Number of nodes cross-stream
Nu	Nusselt Number
p	Pressure, N/m^2
Δp_{cp}	Average pressure drop between corresponding planes
Pe	Peclet number ($Pe = RePr$)
Pr	Prandtl number
$\dot{q}''_{cell}$	Average heat flux into cell, W/m^2-s
$\dot{q}''_p$	Imposed heat flux on plate, W/m^2-s
$\dot{q}''_w$	Local heat flux at fluid-plate interface, W/m^2-s
Re	Reynolds number
s	Rib separation

NOMENCLATURE--Continued

Symbol	Definition
S_x'''	Momentum source in x-momentum equation, N/m^3
S_y'''	Momentum source in y-momentum equation, N/m^3
S_T'''	Energy source in energy equation, W/m^3
T	Temperature, °C
u	Velocity in x-direction, m/s
v	Velocity in y-direction, m/s
w	Rib width, m
x	Cartesian co-ordinate direction
y	Cartesian co-ordinate direction
y_{ℓ}	Distance from centerline to plate wall, m
y_p	Thickness of plate, m
ρ	Density, kg/m^3
μ	Viscosity, kg/m-s
γ_m	Tolerance of core computer program
γ_v	Overall computer program tolerance
ν	Kinematic viscosity, m^2/s
Λ	Resistance coefficient

Subscripts

av	Average value
b	Boundary value
B	Bulk value
f	Fluid value
i	Nodal index

NOMENCLATURE--Continued

Subscripts

Symbol	Definition
int	Internal plane value
	Nodal index
p	Plate value
w	Wall or local value

Superscripts

a	Denotes plane immediately upstream of corresponding plane
b	Denotes plane immediately downstream of corresponding plane
^	Correction value
-	Non-dimensionalized value
*	Estimated value

CHAPTER 1

INTRODUCTION

When studying the flow in ducts, there arise some problems for which a numerical finite-difference method is the only means of obtaining a solution, albeit approximate. One class of such problems, important for the convective heat transfer in advanced concepts for shipbound propulsion, concerns flow downstream of the entry region in two-dimensional ducts with repeating geometry.

The repetition of a geometrical characteristic is outlined in Fig. 1-1. The two-dimensional duct is formed by a pair of parallel plates with square ribs fastened to the surfaces perpendicular to the flow. A rib on one surface opposes a counterpart on the other surface.

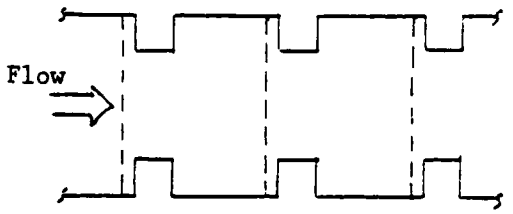

Fig. 1-1. Duct with Repeating Geometry

This duct can be divided into geometric units which are identical to one another. The vertical dashed lines separate the duct segment in Fig. 1-1 into two identical geometric units which will be referred to as 'cells' in the remainder of this report.

Established flow is considered attained when the flow pattern in any cell is independent of the entry region effects and identical to the flow in cells upstream and downstream of itself. It is hypothesized the repeating geometry produces a repeated flow pattern, i.e., a spatially periodic flow.

This report deals with the development and application of a numerical technique incorporating a general computer program for two-dimensional, recirculating flows to produce a solution for the flow in such cells. Since the cell flow pattern may be assumed representative of the flow in the duct beyond the entrance region, ducts whose L/D_h ratio is large may have their dominant pressure drop and heat transfer characteristics predicted by a cell solution. Solving for the flow in a cell rather than a more extensive solution involving the entrance region then becomes an attractive means for obtaining useful engineering information at reduced computational costs.

The numerical technique developed in this report will be applied to two problems. The first problem is concerned with flows in corrugated channels and fractures; the second problem is concerned with flows between ribbed parallel plates. These problems will be titled by the names of the computer programs developed to solve them: CRACFLO and RUFF respectively.

1.1 Problem Statement for CRACFLO

For compact heat exchangers using plate-fin geometrics, one means of augmenting heat transfer is use of a corrugated surface for the plate [Kays and London, 1964]. This geometry is sketched in Figure 1-2.

Studies of heat exchangers with corrugated wall channels are few in number. General friction factors and Nusselt numbers for a single corrugated wall channel geometry are presented by Belabarodov and Volgin [1971]. The friction factors were determined for a Reynolds number range of 5000 to 45,000. The Nusselt numbers were found for $4000 \leq Re \leq 45{,}000$. A definition of the Reynolds number was not provided in the paper.

Two other papers [Goldstein and Sparrow, 1975 and 1977] investigate the mass and heat transfer in corrugated wall channels. The investigations limit study to the first two cycles of the corrugated channel beyond the entrance and do not provide pressure drop or friction factor data. The range of Reynolds numbers in these studies was from 150 to 8550 where

$$Re = \frac{2 H U_B}{\nu} \qquad (1\text{-}1)$$

The symbol H is the maximum channel width as shown in Figure 1-2 (c). Only one geometry was investigated.

Data for three corrugated wall geometries are presented by Kays and London, [1964]. Average friction factors and Stanton-[Prandtl] $^{2/3}$

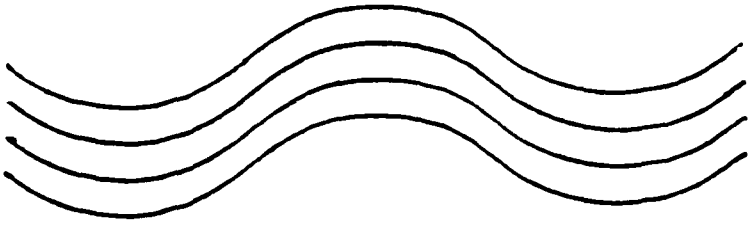

See Fig. 4-11

a) Plate-fin heat exchanger geometry with corrugated surface

b) Conceptualized fracture

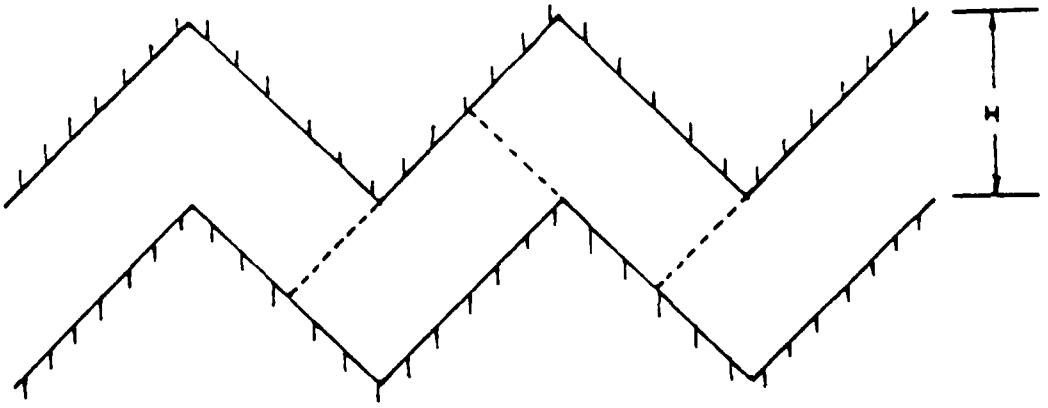

c) Corrugated wall channel

Fig. 1-2. Conceptualized Fracture and Corrugated Wall Channel Schematics

number products are presented for the Reynolds number range of 300 to 10,000. The Reynolds number is based on a hydraulic diameter defined by:

$$D_h = \frac{4 \text{ (minimum flow area) (streamwise length)}}{\text{(transfer surface area)}} \qquad (1\text{-}2)$$

This brief review represents the sum of the literature on corrugated wall channels located by the author. Very few geometries have been studied and the data are incomplete as average friction factors have not even been presented for laminar flow in all cases.

A related problem is the flow in fractures. There arises, on occasion, a need or desire for average friction factor versus Reynolds number or average friction factor versus geometry relationships for fractures and cracks. One such case is for cracks which may occur in pressurized components of power systems [Button et al., 1978].

A crack in a pressurized component is a warning of impending failure. If gases escaping through this crack may be detected, an early warning of the component's failure is available. The construction of a leak detector to serve as a warning device requires an estimate to be made of the leak rate of gases through a crack. The leak rate is dependent on, among other things, the average friction factor.

Flow in rock fractures is another case where the prediction of the average friction factor is desirable. The Dry-Rock geothermal project is a means for extracting energy by circulating water in a fracture system in hot, dry rock deep below the surface of the earth [McFarland,

1975]. The overall flow impedance of the fracture system is important since it determines the pumping power required to flow water through the fracture system. The local fracture impedance has importance when investigating the circulation patterns of the flow.

Two prediction methods available [McFarland, 1975; McFarland and Murphy, 1976] use the D'Arcy relation for hydraulic diffusion to simplify the governing equations. The D'Arcy relation is based on a friction factor-Reynolds number relationship similar to that for laminar flow between parallel plates. Nemat-Nasser and Ohtsubo [1978] assumed a laminar parabolic profile to occur across the fracture gap, neglecting the rough character of the surface.

Therefore, current predictions of flow patterns in cracks and, consequently, the extraction of thermal energy from them are based on a simplified model of the local fracture impedance. It is desirable to determine the local fracture impedance more realistically to improve the accuracy of predictions.

The local flow in a fracture may be assumed to exhibit two-dimensional behavior in regions suitably far removed from the inlet or outlet. Fractures do not exhibit repeating geometry, but have the potential for their average characteristics to be approximated by a repeating geometry. A conceptualized fracture and corrugated wall channel are shown in Figure 1-2. An approximation of the fracture may be achieved through careful selection of a corrugated wall channel geometry. The

average characteristics of a crack or fracture may then be estimated by performing a numerical solution of the flow in a cell of the corrugated wall channel.

Therefore, it is desirable to obtain an understanding of the flow of fluids within a corrugated wall channel. Furthermore, since flow in compact heat exchangers and fractures is often in the laminar flow regime, a solution for laminar flow is sought. Program CRACFLO has been developed to provide a solution for established, laminar flow in corrugated wall channels and, in particular, to provide average friction factors based on calculated pressure drops.

Program CRACFLO utilizes two geometric units or cells. These cells are shown in Figure 1-2 (b) delimited by the dashed lines. The two cell section is shown rotated 45 degrees clockwise in Figure 1-3. Characteristic dimensions given in this figure are g, the channel gap width, and a, the distance between the corner regions. The geometric restrictions for this problem are: 1) the corrugations must include 90 degrees, i.e., square corners and 2) the distance between the corner regions, a, cannot be less than zero.

To enable modeling of many possible fracture geometries, the length a is variable while g is held constant. The geometry is then characterized by the ratio a/g. The flow is characterized by a Reynolds number

$$Re = \frac{\rho U_B g}{\mu} \qquad (1\text{-}3)$$

where U_B represents the bulk velocity through the duct.

Due to the unique geometry, the corresponding planes in Figure 1-3 do not separate cells whose flow patterns are identical, but rather are mirror images of each other. Computational difficulties or an invalidation of the assumptions of periodic flow do not result, however. The application of the periodic boundary conditions to this problem will be discussed in the Analysis section.

1.2 Problem Statement for RUFF

The usage of artificially roughened surfaces for enhancing heat transfer has been under investigation for some time [Bergeles, 1978]. This report will be concerned with a type of roughness referred to as transverse or repeated ribs.

The ribs are rectangular in shape and affixed to, or integral with, a flat plate. The geometry to be investigated is similar to that shown in Figure 1-4. The dimensions shown are the rib height, h, the rib length, l, the rib separation, s, the plate thickness, y_p, and the wall to centerline distance, y_{ℓ}.

Though considerable data exist for repeated rib roughness, there remains uncertainty in predicting the performance of a particular repeated rib surface. There have been attempts to reduce data to a general correlation [Webb, 1978] and to provide a means for optimizing a roughness configuration, [Lewis, 1975 a,b]. These methods, however, provide the designer with average characteristics of the rough surfaces and have their own uncertainties.

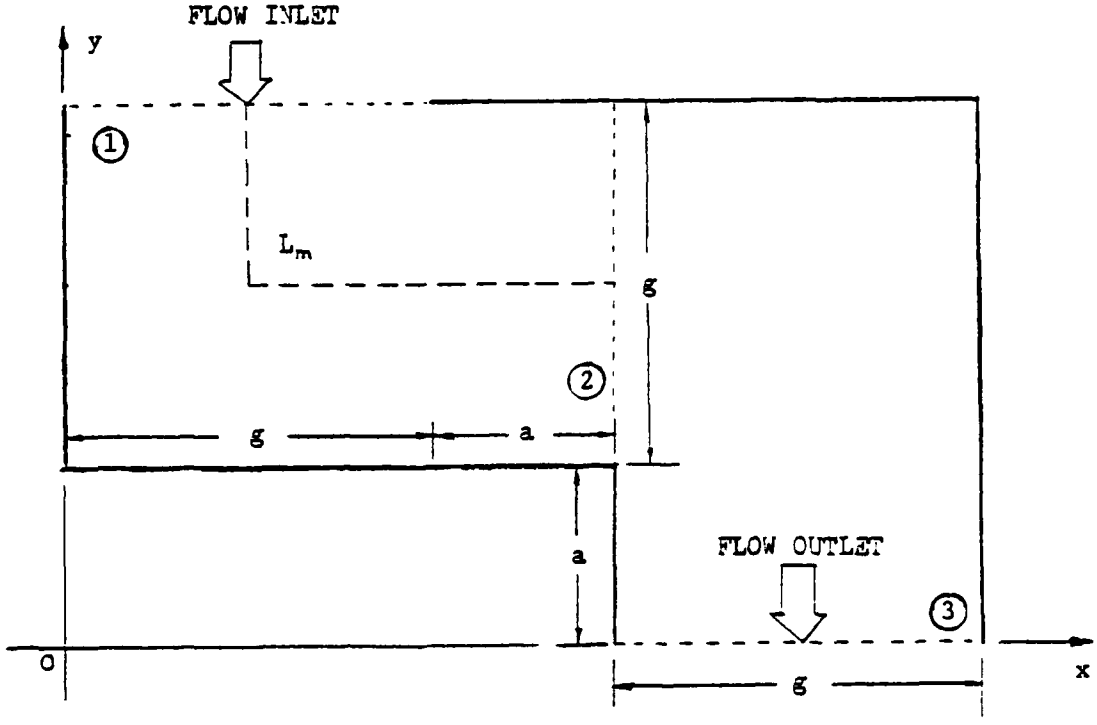

Fig. 1-3. Schematic for Corrugated Duct Representative Cell

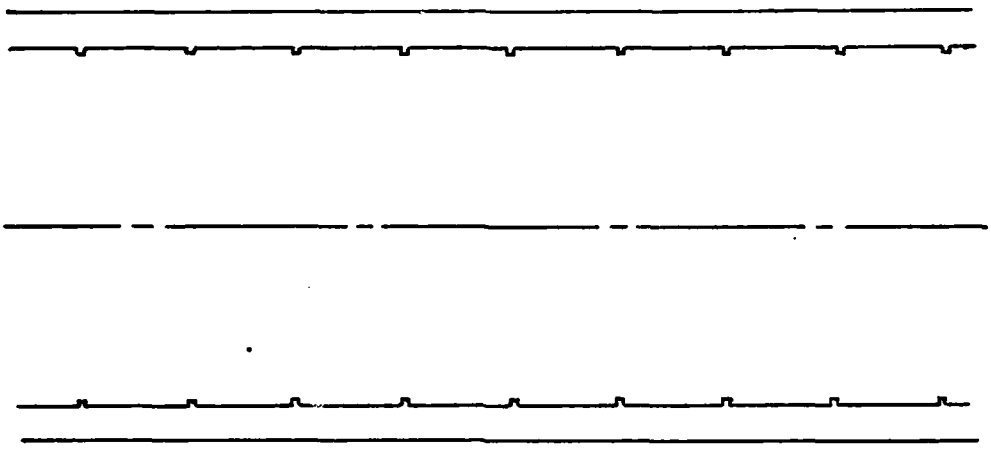

a) Overview Schematic

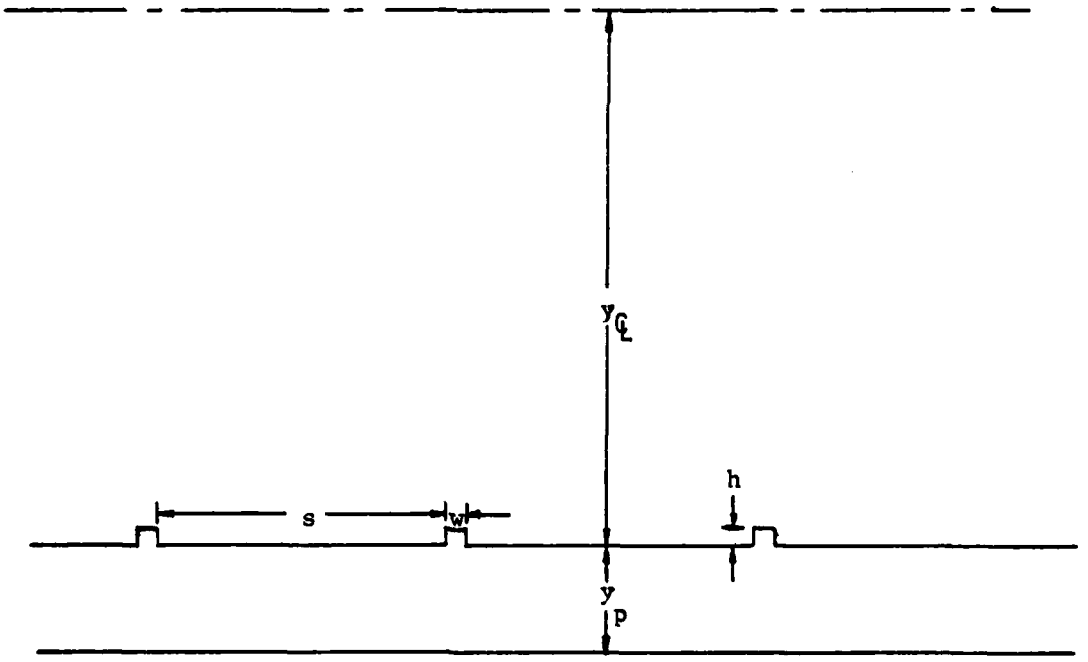

b) Dimensioned Schematic

Fig. 1-4. General Drawings for a Repeating Rib Geometry

A heat exchanger designer may desire knowledge of the local values of the Nusselt number and where potential hot spots may occur. Additionally, the designer may wish to have a convenient means of prediction and optimization at his disposal in order to allow him to survey many designs without laborious usage of graphs, correlations or experiments.

A general numerical program is potentially a convenient means of prediction and optimization. The program may be constructed to provide the detailed information the designer may desire as well. The overall performance of a repeated-rib surface may be estimated by a numerical solution of the flow and heat transfer in a cell if the entry region is of negligible overall importance. Detailed information for much of the duct may be provided as well.

This report continues an effort to develop a numerical program solving for the flow and heat transfer in a cell begun by Short [1977]. The latest program to be developed is titled program RUFF.

Program RUFF utilizes a two cell approach as described in Chapter 3 and solves only for constant property, laminar, incompressible flow. The solution domain is shown in Figure 1-5. This figure is approximately to the scale of a planned experiment. Since the duct shown in Figure 1-4 is symmetric about the centerline, it is only necessary to solve from the wall to the centerline. The energy equation is solved both in the fluid and the plate.

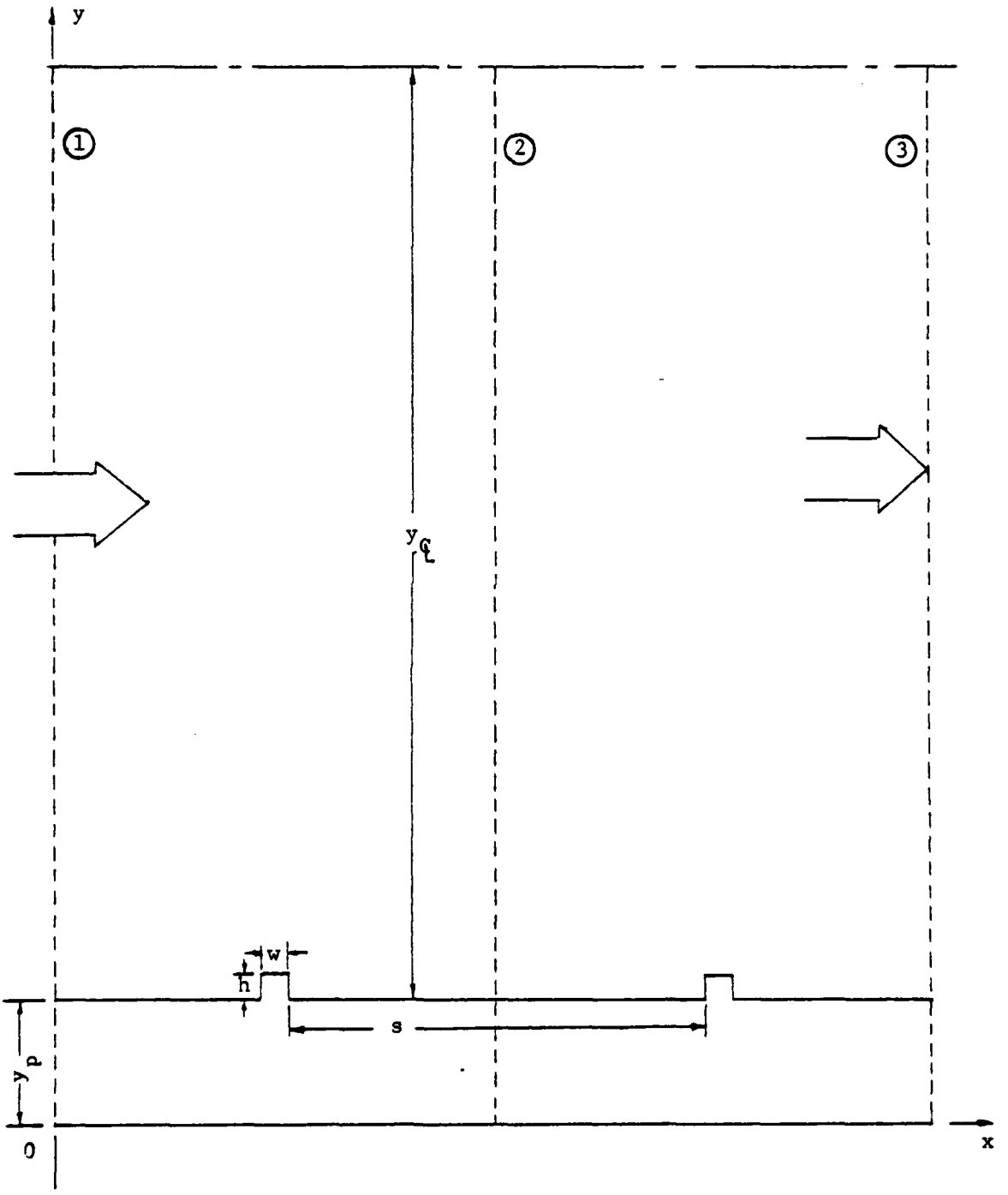

Fig. 1-5. Solution Domain for Program RUFF

Extensions beyond Short's work include calculation of local friction factors and Nusselt numbers, a more flexible scheme for assigning the numerical grid - allowing easier geometry definition - and a stable solution method.

CHAPTER 2

ANALYSIS

2.1 Governing Equations

The problems considered in this report are assumed to involve steady state, recirculating, laminar incompressible flows with constant properties. The fluid medium is presumed to be a Newtonian fluid.

The governing equations for the CRACFLO and RUFF program in a cartesian coordinate system are:

Continuity:

$$\frac{\partial u}{\partial x} + \frac{\partial v}{\partial y} = 0 \tag{2-1}$$

X-momentum:

$$\rho \left[u \frac{\partial u}{\partial x} + v \frac{\partial v}{\partial y} \right] = - \frac{\partial p}{\partial x} + \mu \left[\frac{\partial^2 u}{\partial x^2} + \frac{\partial^2 u}{\partial y^2} \right] + \dot{S}_x''' \tag{2-2}$$

Y-momentum:

$$\rho \left[u \frac{\partial v}{\partial x} + v \frac{\partial v}{\partial y} \right] = - \frac{\partial p}{\partial y} + \mu \left[\frac{\partial^2 v}{\partial x^2} + \frac{\partial^2 v}{\partial y^2} \right] + \dot{S}_y''' \tag{2-3}$$

Energy:

$$\rho c_p \left[u \frac{\partial T}{\partial x} + v \frac{\partial T}{\partial y} \right] = k \left[\frac{\partial^2 T}{\partial x^2} + \frac{\partial^2 T}{\partial y^2} \right] + \dot{S}_T''' \tag{2-4}$$

It has been assumed in the energy equation that viscous dissipation is negligible.

The governing equations are solved such that conditions of periodicity as described by Short [1977] and separately by Patanker, Liu and Sparrow [1977] are imposed.

2.2 Equation Non-Dimensionalization

Problem CRACFLO

The non-dimensionalization of the momentum equations for problem CRACFLO will be illustrated using the x-momentum equation. The non-dimensional variables are:

$$\bar{x} = \frac{x}{g} \qquad \bar{\rho} = \frac{\rho}{\rho U_B^2}$$

$$\bar{y} = \frac{y}{g} \qquad \bar{U} = \frac{U}{U_B} \qquad (2\text{-}5)$$

$$\bar{v} = \frac{v}{U_B}$$

Introducing equations 2-5 into equation 2-2 yields

$$\bar{U}\frac{\partial \bar{U}}{\partial \bar{x}} + \bar{v}\frac{\partial \bar{U}}{\partial \bar{y}} = -\frac{\partial \bar{p}}{\partial \bar{x}} + \frac{1}{Re}\left[\frac{\partial^2 \bar{U}}{\partial \bar{x}^2} + \frac{\partial^2 \bar{U}}{\partial \bar{y}^2}\right] + \frac{\dot{S}_x''' g}{\rho U_B^2} \qquad (2.6)$$

where the Reynolds number is

$$Re = \frac{\rho U_B g}{\mu} \qquad (2.7)$$

The controlling parameters in problem CRACFLO may now be seen to be the Reynolds number and the geometry ratio, a/g.

Problem RUFF

The non-dimensionalization of the momentum equations for problem RUFF will be illustrated using the x-momentum equation. The non-dimensional variables are:

$$\bar{x} = \frac{x}{y_{\text{℄}}} \qquad \bar{p} = \frac{p}{\rho U_B^2}$$

$$\bar{y} = \frac{y}{y_{\text{℄}}} \qquad \bar{U} = \frac{U}{U_B} \qquad (2\text{-}8)$$

$$\bar{v} = \frac{v}{U_B}$$

Introducing equations 2-8 into equation 2-2 yields

$$U \frac{\partial \bar{U}}{\partial \bar{x}} + \bar{v} \frac{\partial \bar{U}}{\partial \bar{y}} = - \frac{\partial \bar{p}}{\partial \bar{x}} + \frac{1}{Re} \left[\frac{\partial^2 \bar{U}}{\partial \bar{y}^2} + \frac{\partial^2 \bar{U}}{\partial \bar{y}^2} \right] + \frac{\dot{s}'''_{\text{℄}}}{\rho U_B^2} \qquad (2\text{-}9)$$

where

$$Re = \frac{\rho U_c y_{\text{℄}}}{\mu} \qquad (2\text{-}10)$$

The energy equation is non-dimensionalized using equations 2-8 and the non-dimensional expression for temperature:

$$\bar{T} = \frac{T - T_o}{\dot{q}''_p y_{\text{℄}} / k_f} \qquad (2\text{-}11)$$

where $\dot{q}_p''$ is the imposed heat flux, y_{ℓ} the distance from the plate wall to the centerline and k_f the fluid thermal conductivity. The non-dimensional energy equation in the fluid is

$$\bar{u}\frac{\partial\bar{T}}{\partial\bar{x}} + \bar{v}\frac{\partial\bar{T}}{\partial\bar{y}} = \frac{1}{Re\ Pr}\left[\frac{\partial^2\bar{T}}{\partial\bar{x}^2} + \frac{\partial^2\bar{T}}{\partial\bar{y}^2}\right] + \frac{\dot{S}_T'''k_f}{\rho c_p U_B \dot{q}_p''} \tag{2-12}$$

The non-dimensional energy equation in the plate is different:

$$0 = \frac{k_p/k_f}{Re\ Pr}\left[\frac{\partial^2\bar{T}}{\partial y^2} + \frac{\partial^2\bar{T}}{\partial\bar{y}^2}\right] \frac{\dot{S}_T'''k_f}{\rho c_p U_B \dot{q}_p''} \tag{2-13}$$

The controlling parameters that describe problem RUFF are seen to be: the Reynolds number, the Prandtl number, the duct geometry and the ratio, k_p/k_f.

All planar sources of heat such as $\dot{q}_p''$ or $\dot{q}_w''$ are non-dimensionalized as follows:

$$\bar{\dot{q}}'' = \frac{\dot{q}''/\dot{q}_p''}{Re\ Pr}$$

2.3 Boundary Conditions for CRACFLO

Two solution cells for the CRACFLO program are shown in Figure 1-3. The corresponding planes are shown in dotted lines and are numbered 1, 2 and 3. The heavy solid lines represent impermeable, stationary boundaries.

For the solid boundaries, the no-slip boundary conditions

$$u_{boundary} = 0$$
$$v_{boundary} = 0 \tag{2-14}$$

are applied.

It is necessary to hypothesize the form of the velocity solution to provide boundary conditions at the corresponding planes 1, 2 and 3. For a two-dimensional duct, we hypothesize the velocity solution to be

$$\vec{u}(x,y) = \vec{u}(x,y)_{\substack{\text{entry}\\\text{region}}} + \vec{u}(x,y)_{\text{periodic}} \tag{2-15}$$

Since we are interested only in the solution for the established velocity field where the effects of $\vec{u}(x,y)_{\substack{\text{entry}\\\text{region}}}$ are negligible, it is $\vec{u}(x,y)_{\text{periodic}}$ which provides the boundary conditons.

Periodic flow in this case means steady flow with time, but periodic in space. That is, the flow in one solution cell is identical to the flow in all other cells beyond the entry region. The corresponding planes separate the duct into solution cells. At these corresponding planes, the hypothesis of periodic, established flow results in the following conditions which must be met for the CRACFLO problem:

$$\begin{aligned}
&-v(x,g+a) = u(g+a,\ g+a-x) = -v(x+g+a,0)\\
&-u(x,g+a) = v(g+a,\ g+a-x) = -u(x+g+a,0)\\
&\frac{\partial v}{\partial y}(x,g+a) = \frac{\partial v}{\partial x}(g+a,\ g+a-x) = \frac{\partial v}{\partial y}(x+g+a,0)\\
&\frac{\partial u}{\partial x}(x,g+a) = \frac{\partial v}{\partial y}(g+a,\ g+a-x) = \frac{\partial u}{\partial x}(x+g+a,0)
\end{aligned} \tag{2-16}$$

These conditions cannot be imposed directly because the velocities and gradients are unknown and must be determined as part of the solution procedure.

The energy equation is not solved in CRACFLO, thereby removing the need for boundary conditions on it.

2.4 Boundary Conditions for RUFF

Two solution cells are shown for program RUFF in Figure 1-5. The heavy solid lines denote stationary, impermeable boundaries and the dotted lines represent corresponding planes.

For the solid boundaries, the no slip boundary conditions,

$$u_{boundary} = 0$$
$$v_{boundary} = 0 \qquad (2\text{-}17)$$

are applied at the fluidplate interface. At the external edge of the plate ($y = 0$) a prescribed heat flux, $\dot{q}''_p$, is imposed.

At the centerline, we impose conditions of symmetry:

$$\frac{\partial U}{\partial y}(x, y_{\ell} + y_p) = 0$$
$$\frac{\partial v}{\partial y}(x, y_{\ell} + y_p) = 0 \qquad (2\text{-}18)$$
$$\frac{\partial T}{\partial y}(x, y_{\ell} + y_p) = 0$$

To provide boundary conditions at the corresponding planes, it is necessary to hypothesize the form of the velocity and temperature solution [Short, 1977]. We may hypothesize solutions such as:

$$\vec{u}(x,y) = \vec{u}(x,y)_{\substack{\text{entry}\\\text{region}}} + \vec{u}(x,y)_{\text{periodic}}$$
$$T(x,y) = T(x,y)_{\substack{\text{entry}\\\text{region}}} + mx + T(x,y)_{\text{periodic}} \qquad (2\text{-}19)$$

The term mx in the temperature distribution accounts for the continuous increase in temperature level due to the imposed heat flux.

Since we are interested in established flow where the effect of the entry region term is negligible, equations (2-19) become:

$$\begin{aligned} \bar{u}(x,y)_{\substack{\text{fully}\\\text{developed}}} &= \bar{u}(x,y)_{\text{periodic}} \\ T(x,y)_{\substack{\text{fully}\\\text{developed}}} &= mx + T(x,y)_{\text{periodic}} \end{aligned} \tag{2-20}$$

The spatially periodic condition of the velocities implies that flow in one solution cell is identical to the flow in all other solution cells beyond the entrance region. The postulated periodic flow yields the remaining boundary conditions for the two momentum equations:

$$u(0,y) = u(s+w,y) = u(2s+2w,y) \tag{2-21a}$$

$$v(0,y) = v(s+w,y) = v(2s+2w,y) \tag{2-21b}$$

$$\frac{\partial u}{\partial x}(0,y) = \frac{\partial u}{\partial x}(s+w,y) = \frac{\partial u}{\partial x}(2s+2w,y) \tag{2-21c}$$

$$\frac{\partial v}{\partial x}(0,y) = \frac{\partial v}{\partial x}(s+w,y) = \frac{\partial v}{\partial x}(2s+2w,y) \tag{2-21d}$$

The boundary conditions for the energy equation follow from much the same reasoning, except the addition of energy must be treated. Since energy is being added to the fluid, the bulk temperature of the fluid is continuously rising so it is impossible to relate scalar temperatures in the same manner as scalar velocities, equations (2-21a) and (2-21b).

As a result of a constant heat flux applied to the exterior of the plate, the bulk temperature of the fluid increases almost linearly, leading to the term, mx, in the hypothesized temperature solution. The conditions of periodic flow yield as a consequence identical temperature

profiles at corresponding planes when the temperatures are non-dimensionalized by the difference between the bulk fluid temperature and the wall temperature at these planes

$$\left.\frac{T - T_w}{T_B - T_w}\right|_{①} = \left.\frac{T - T_w}{T_B - T_w}\right|_{②} = \left.\frac{T - T_w}{T_B - T_w}\right|_{③} \tag{2-22}$$

We know that the bulk temperatures of the fluid are related linearly between any two corresponding planes, i.e.,

$$\begin{aligned} T_{B②} &= T_{B①} + m(s + w) \\ T_{B③} &= T_{B①} + m(2s + 2w) \end{aligned} \tag{2-23}$$

If we were to assume that T, and T_w are also linearly related by the same constant, m, equation (2-22) is satisfied identically. It is the condition of all temperatures at corresponding planes being linearly related that will be used to provide one streamwise boundary condition on the energy equation:

$$T(0,y) = T(s + w,y) - m(s + w) = T(2s + 2w,y) - m(2s + 2w) \tag{2-24}$$

Another boundary condition at the corresponding planes is provided by differentiating equation (2-24) with respect to x

$$\frac{\partial T}{\partial x}(0,y) = \frac{\partial T}{\partial x}(s + w,y) = \frac{\partial T}{\partial x}(2s + 2w,y) \tag{2-25}$$

CHAPTER 3

NUMERICAL TECHNIQUE

The primary difficulty in solving problems with periodic boundary conditions is that the values of velocity and temperature on the upstream and downstream corresponding planes are unknown. Typically all values and/or fluxes are known on the boundaries in numerical problems. This chapter concerns itself with the method used in programs CRACFLO and RUFF to impose periodic boundary conditions.

3.1 History

There are a number of numerical techniques to impose periodic boundary conditions. All methods have a common action. The methods act upon those boundary velocities which are subject to periodic boundary conditions in an orderly fashion seeking those boundary values which are correct according to the physics of the problem. The boundary temperatures are similarly treated in cases where the energy equation is solved.

A total of five methods have been investigated by the author. These will be briefly described in the chronological order of their investigation. The term "updating," used in the following discussion is defined as any rational process by which the upstream and downstream boundary conditions are altered in an attempt to affect a solution.

The first technique was the one-cell successive substitution method of Short [1977]. This method was found to be unstable in the

sense that it produced a divergent solution. Later, this instability was determined to be due to updating the upstream and downstream boundary conditions every iteration.

The second technique was a sensitivity matrix method invented by the author but related to Newton's method [Cebeci and Bradshaw, 1977, sec. 4.2.2]. This method utilized a matrix of sensitivity coefficients produced by perturbing a test flow field for a particular geometry. The sensitivity matrix provided linear relationships between changes in the boundary velocity values and changes in the velocities on the internal plane. These relationships furnished a means of updating to obtain periodic boundary conditions. The sensitivity matrix method required more accuracy and execution time of the computer program than appeared economically feasible.

The third technique was the internal plane method. This method utilizes the velocities on the internal plane directly to provide new values on the boundary planes. This method is stable and applicable to both the CRACFLO and RUFF problems. One drawback is the requirement for considerable execution time. However, this method was selected to solve the CRACFLO and RUFF problems, partly due to its reliability.

The fourth technique is called a stabilized one-cell successive substitution method. This is the method of Short [1977], stabilized by updating only every ten iterations. Though the solution domain is half that of the internal plane update method, execution time is greater due to a lower convergence rate.

The fifth technique is that of Patankar, Liu and Sparrow [1977]. This method utilizes a cyclic tridiagonal matrix in the streamwise direction to impose periodic boundary conditions directly as part of the solution of the finite difference equations rather than separately as is done in the first four methods. The author was unable to construct an operable version of this method for testing. While the application of this method to CRACFLO presents difficulties, the cyclic tridiagonal matrix method may be an excellent alternative for RUFF. However, since the TEACH program uses an upwind differencing procedure for strong convection, this technique may not be effective when there is dominant outflow at the downstream boundary. The Internal Plane Method, abbreviated IPM, will now be discussed in detail. The other four methods are covered in more detail by Faas [1979; Appendix D].

3.2 Internal Plane Method

The IP method is, in a sense, a fusion of the method of Short [1977] and certain elements of the sensitivity matrix method mentioned above. The IP method uses two cells sharing a common corresponding plane and requires the external corresponding planes to have identical scalar values of velocity. It also uses the internal plane to provide information leading to the estimation of new boundary values.

The IP method will be treated in detail using the solution domain of program CRACFLO as an example. The geometry is repeated in Fig. 3-1. The dotted lines numbered 1, 2 and 3 are the corresponding planes. Planes 1 and 3 are the boundary planes and plane 2 is the internal plane. The internal plane is a mirror image of the boundary planes, with point A corresponding to point A'.

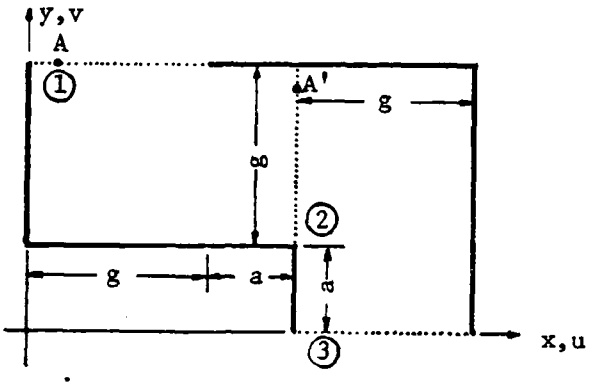

Fig. 3-1. CRACFLO Geometry

The general numerical technique of IPM is to estimate initial values of u and v velocities at the planes 1 and 3 and to solve for the flow field numerically. The influence of the duct geometry as well as the boundary conditions determines the u and v velocities at plane 2. Hence, these u and v velocity values become better estimates of the actual velocity values that satisfy the periodic boundary conditions.

These deduced values are then substituted for the previous boundary velocity values and the process is repeated until periodic boundary conditions are met. The process of starting with a set of boundary values and ending with their replacement with values from the internal plane will be referred to as a "cycle." This process is distinct from an iteration of the core program.

Many details have been omitted above and require further discussion. A simple model using four nodes cross-stream will be used for purposes of illustration. Figure 3-2 shows the location and title of the various pertinent velocities. The subscript "b" denotes a boundary velocity, the subscript "int" an internal plane velocity, the superscript

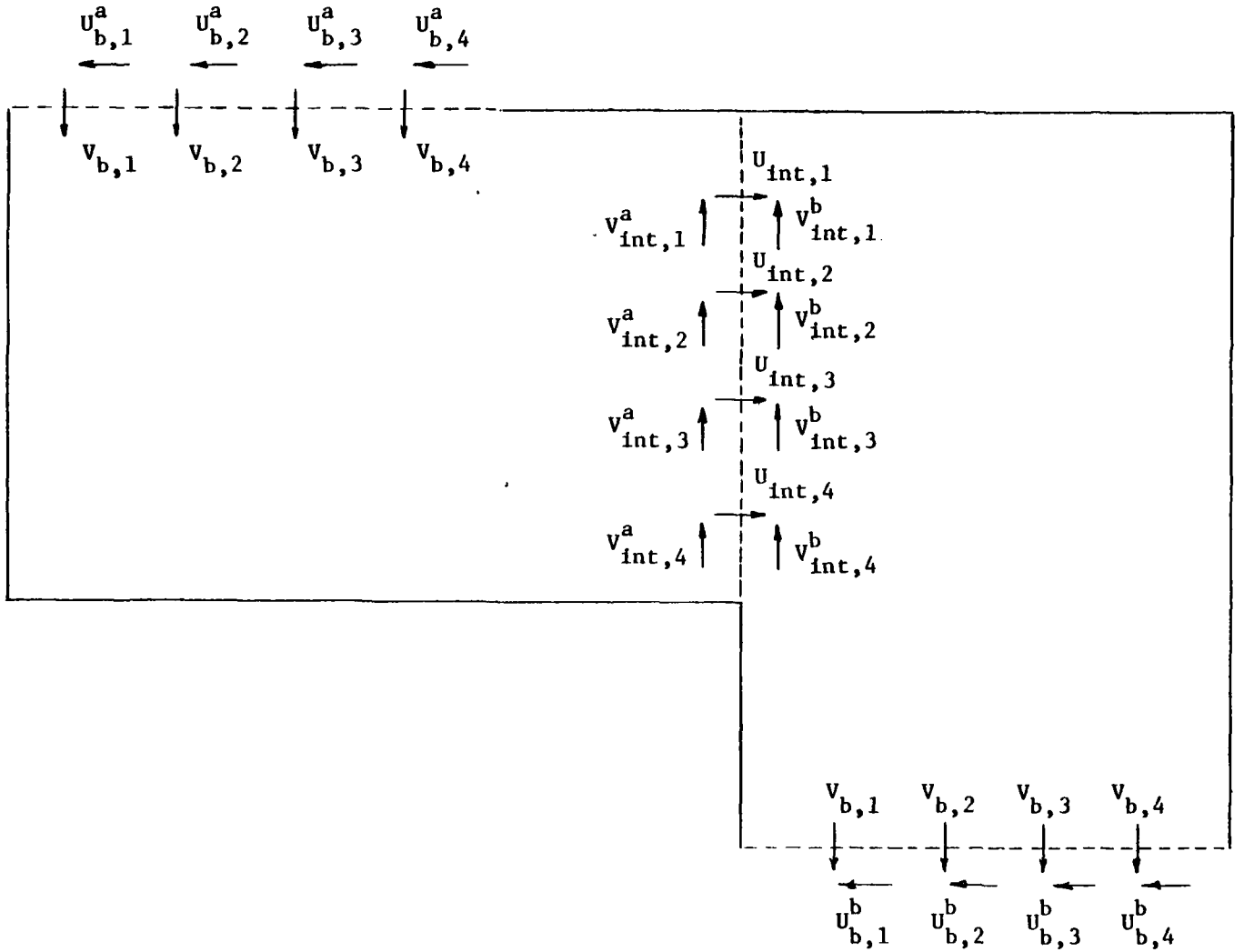

Fig. 3-2. Velocity locations and titles for illustrative example

"a" refers to an upstream boundary, and the superscript "b" to a downstream velocity. The superscripts "a" and "b" are necessary due to the staggered grid utilized by TEACH, the program which is a basis of CRACFLO and RUFF.

The first step taken by program CRACFLO is to initialize the variable fields and the boundary conditions. The u and v velocities are initially set to zero except for the boundary velocities $v_{b,n}$ which are initialized to represent a parabolic velocity profile whose flow direction is the same as shown in Figure 3-2. The subscript "n" may take on the values 1, 2, 3 or 4 in this example.

The core program uses the initial boundary conditions to solve for u and v velocities and pressures within the solution domain until a convergence criterion γm is met.

The core program utilizes a convergence criterion based on the calculated mass flow imbalance over the solution domain. A mass flow imbalance of a nodal control volume is referred to as its residual mass source. The core program is considered converged when the absolute sum of the mass residual sources of the nodal control volumes is less than a certain fraction of the mass flow rate through the solution domain. Mathematically this is

$$\frac{\sum \left| \dot{m}_{\substack{\text{nodal} \\ \text{sources}}} \right|}{\dot{m}_{in}} \leq \gamma m \qquad (3\text{-}1)$$

where γm is the chosen fraction of the mass flow rate.

Core program convergence is complicated by the ability to achieve a desired tolerance value of γm when the estimated boundary velocity values are far from those of periodic flow. This situation is almost always the case for the initial boundary values. This complication is solved by selecting an initial tolerance, γm_{init}, which is sufficiently large to allow convergence to be achieved with initial boundary values. This value is reduced as the program proceeds by a preset constant, R, prior to the commencement of the next cycle. The tolerance is reduced until a minimum tolerance, γm_{min}, is reached or exceeded. The value of γm is then fixed at γm_{min} for all subsequent cycles.

Once the core program has converged, the program then checks for overall convergence. Overall convergence is determined by comparing how well the deduced boundary values satisfy the periodic boundary conditions. Ideally, one condition to be met is

$$-v_b = u_{int} \tag{3-2}$$

where the subscript "b" refers to a value on the boundary planes and the subscript "int" refers to a value on the internal plane. Since the internal plane is rotated 90° with respect to the boundary plane, we must compare u velocities on one plane with v velocities on the other with the appropriate correction of sign.

Experience with the program shows that the streamwise velocities apparently dominate the physics of the flow to such an extent that satisfying equation (3-2) results in the satisfaction of the remaining periodic boundary conditions as detailed in chapter two. This dominance is

exploited to provide overall convergence criteria which are relatively simple to apply. Overall convergence is considered to be achieved when

$$\frac{|v_{b,n}| - |u_{int,n}|}{|v_{b,n}|} \leq \gamma_v \qquad (3\text{-}3)$$

where the subscript "n" refers to a particular corresponding node on the internal and boundary planes and γ_v is a tolerence value. This criterion must be met by every pair of corresponding velocities before overall convergence is considered accomplished. If overall convergence is accomplished, then the program prints the variable arrays and local flow angles then stops. If the convergence criteria are not met, the program proceeds to perform an update of the trial boundary values.

The program numerically integrates the velocity profile at the internal plane to determine the mass flow rate, $\dot{m}_{int}$, across it. A flow correction factor, F_c, is calculated by

$$F_c = \frac{\dot{m}_{ref}}{\dot{m}_{int}} \qquad (3\text{-}4)$$

where $\dot{m}_{ref}$ is calculated from the Reynolds number and fluid properties.

Next the velocities at the internal plane are used to replace those at the boundaries as follows:

$$v_{b,1} = -F_c\, u_{int,1} \qquad (3\text{-}5)$$

$$u^a_{b,1} = -v^a_{int,1} \qquad (3\text{-}6)$$

$$u^b_{b,1} = -v^b_{int,1} \qquad (3\text{-}7)$$

$$v_{b,2} = -F_c\, u_{int,2} \qquad (3\text{-}5)$$

$$u^a_{b,2} = -v^a_{int,2} \qquad (3\text{-}6)$$

$$u^b_{b,2} = -v^b_{int,2} \qquad (3\text{-}7)$$

$$v_{b,3} = -F_c\, u_{int,3} \qquad (3\text{-}5)$$

$$u^a_{b,3} = -v^a_{int,3} \qquad (3\text{-}6)$$

$$u^b_{b,3} = -v^b_{int,3} \qquad (3\text{-}7)$$

$$v_{b,4} = -F_c\, u_{int,3} \qquad (3\text{-}5)$$

$$u^a_{b.4} = -v^a_{int,4} \qquad (3\text{-}6)$$

$$u^b_{b,4} = -v^b_{int,4} \qquad (3\text{-}7)$$

where it may be seen the purpose of F_c is to scale the velocity profile at the internal plane to conserve the overall mass flow rate.

The correction factor, F_c, is printed every update as an indication of how the solution procedure is working. The correction factor should approach a constant value of one as the program moves toward overall convergence. This is observed in all cases.

The program then reduces the value of the core program convergence criteria, γ_m, by a factor of R. If this results in the value of γ_m being reduced below a minimum value, γm_{min}, the value of γ_m is set to γm_{min}.

The core program then solves for the u and v velocities and pressures with the new boundary values on the boundary planes. The process is repeated until overall convergence is reached. A flow chart of the entire process is shown in Figure 3-3.

3.3 Application of the IP Method to RUFF

The IP technique is applied to RUFF in a straight-forward fashion comparable to CRACFLO insofar as the velocities are concerned. Additional calculations are required to enforce periodic boundary conditions on the energy equation as detailed in chapter two.

Overall convergence of RUFF is reached when the following is attained

$$\frac{|u_{b,n} - u_{int,n}|}{|v_{b,n}|} \leq \gamma_v \qquad (3\text{-}8)$$

In order to maintain a constant mass flow rate, the streamwise velocities are corrected at each update by a correction factor F_c as

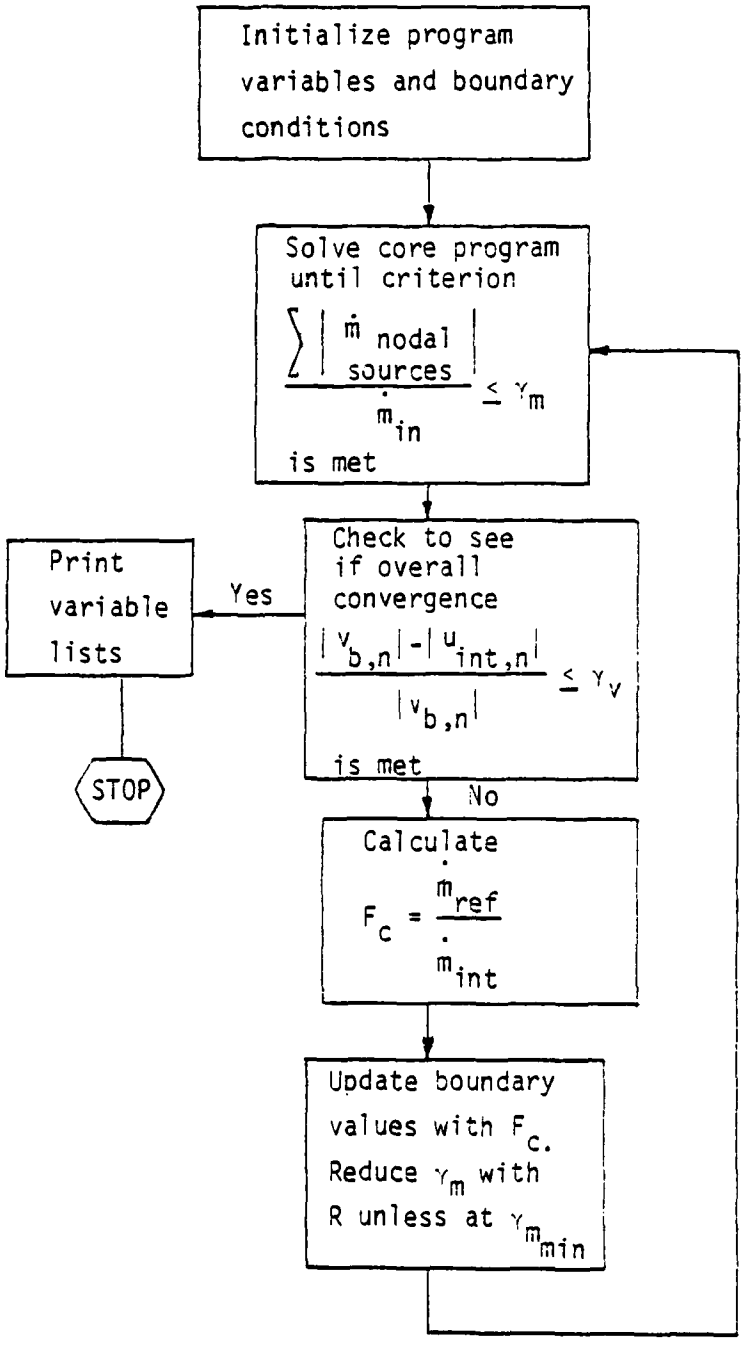

Fig. 3-3. General Flowchart for CRACFLO

defined in equation (3-4). The update performed is shown below

$$u_{b,n} = F_c \, u_{int,n} \tag{3-9}$$

$$v^a_{b,n} = v^a_{int,n} \tag{3-10}$$

$$v^b_{b,n} = v^b_{int,n} \tag{3-11}$$

The superscripts "a" and "b" refer to the upstream and downstream boundary and internal values respectively as related in the CRACFLO example and shown in Figure 3-4.

A constant heat flux is applied to the outer edge of the ribbed plate in program RUFF. This requires the bulk temperature of the fluid between corresponding planes to increase with x by the incremental amount, m, defined by

$$\left(\frac{\Delta T_B}{\Delta x}\right)_{cp} = m = \frac{\dot{q}''_p}{\rho c_p U_B y_{\mathcal{C}}} \tag{3-12}$$

where $\dot{q}''_p$ is the imposed heat flux, c_p the fluid specific heat, T_B the bulk temperature of the fluid and U_B the bulk fluid velocity.

The specification of the fluid bulk temperature at any section of the computational cell means the bulk temperature at any corresponding plane of the duct is also specified. Selecting an inlet bulk temperature for an upstream boundary condition automatically determines the bulk temperature at the downstream boundary. These bulk temperatures must remain fixed regardless of the boundary temperature profiles to maintain overall

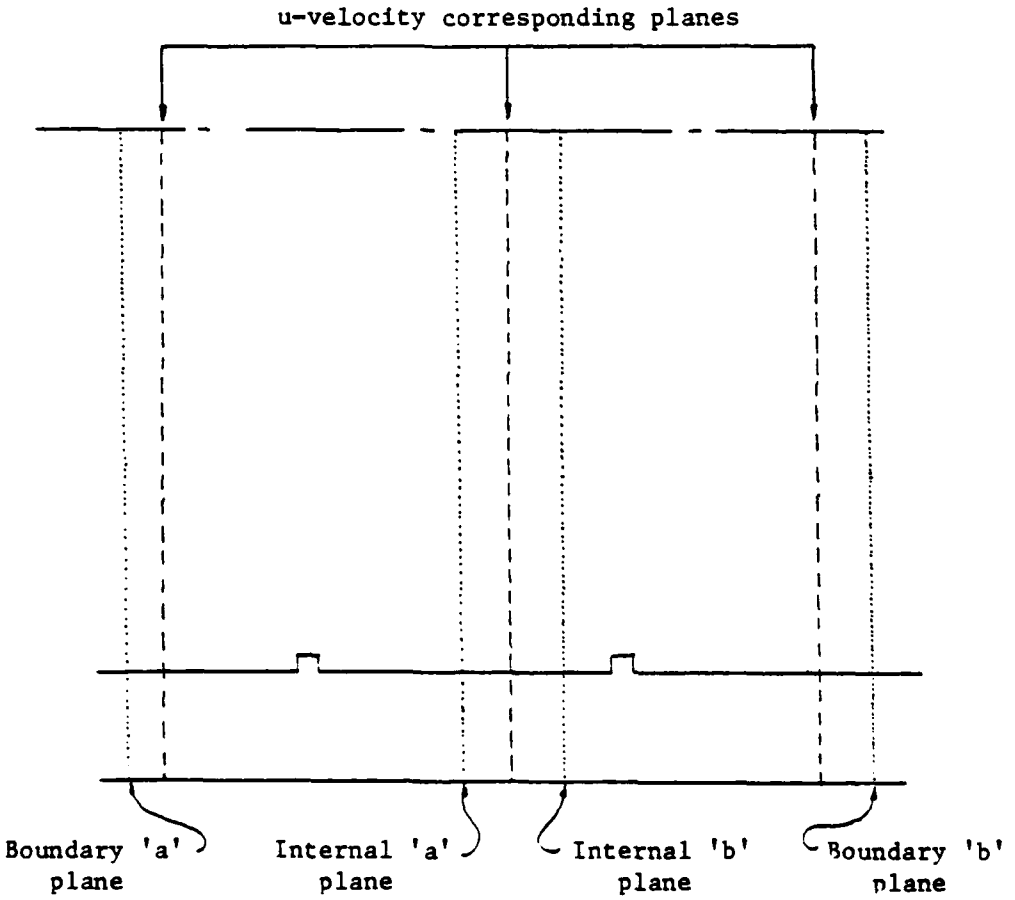

Fig. 3-4. Location of the "a" and "b" Planes

conservation of energy. The boundary temperature profiles are updated such that the inlet and outlet bulk temperatures conserve energy as follows.

When Ruff initializes the temperature field for a particular problem, the bulk temperatures at the two internal corresponding planes, T_{Ba} and T_{Bb}, are recorded. Two internal planes are required for the temperatures as was necessary for the v-velocities because of the staggered grid used in program TEACH.

The energy equation is solved in each cycle after the momentum equations are solved for the velocity field. This is possible since the fluid properties are not temperature dependent in program RUFF; thereby the momentum equations are decoupled from the energy equation. The energy equation is solved to an accuracy where the sum of the individual nodal energy imbalances is less than a specified fraction of the imposed heat transfer through the wall, that is,

$$\sum \left| \dot{q}'_{\substack{\text{nodal} \\ \text{sources}}} \right| \leq \gamma_e \cdot \dot{q}''_p \, \Delta_x \qquad (3\text{-}13)$$

where γ_e is the tolerance fraction and $\Delta_x = 2(S + W)$. (In the present version of the program the units are incorrect on the righthand side due to an oversight when constructing the code. Operationally, this difficulty has had little effect on program performance.)

The temperature profiles at the internal corresponding planes are integrated to determine the bulk temperatures, T_{B1} and T_{B2}, at those planes. Temperature correction factors, T_{C1} and T_{C2}, are then produced using the bulk temperatures, T_{Ba} and T_{Bb}, deduced when RUFF was initialized:

$$T_{c1} = \frac{T_{Ba}}{T_{B1}} \tag{3-14}$$

$$T_{c2} = \frac{T_{Bb}}{T_{B2}} \tag{3-15}$$

The temperature boundary conditions are then updated upstream and downstream by the following process:

$$T^{a}_{B,n} = T_{c1} \cdot T^{a}_{int,n} \tag{3-16}$$

$$T^{b}_{B,n} = T_{c2} \cdot T^{b}_{int,n} \tag{3-17}$$

A general flowchart for RUFF is shown in Figure 3-5.

3.4 Confidence Tests

Program CRACFLO

Several tests of program CRACFLO were conducted to determine a) the uniqueness of the numerical solutions found, and b) the effect of refining the grid mesh. The latter test is also known as a test of grid independence.

When discussing the tests, a convenient way of expressing the grid refinement is by the number of nodes cross-stream, N_N. The number of nodes cross-stream is the number of nodes on a corresponding plane that lie between the solid walls. For example, the number of nodes cross-stream shown in Figure 3-2 is four. (When a particular number of nodes cross-stream is mentioned in the following, the reference is to a specific grid scheme that was used and not to one of many other grid schemes

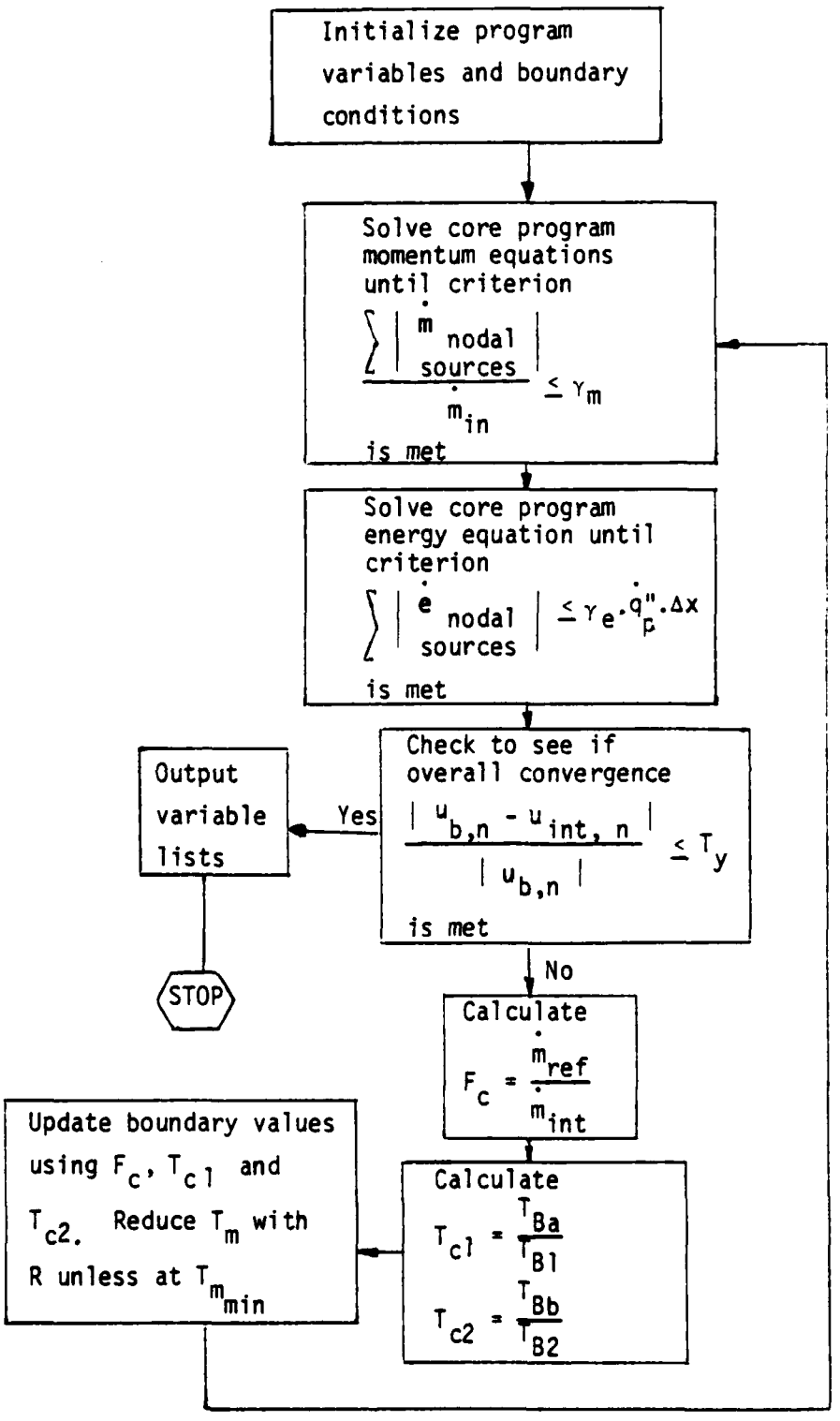

Fig. 3-5. General Flowchart for RUFF

that satisfy the requirement of having the specified number of nodes cross-stream.)

The uniqueness tests were conducted with a grid having 12 nodes cross-stream, a Reynolds number of 100 and a geometry ratio, $a/y = 0.5$. Instead of the usual parabolic profile as initial inlet and outlet boundary velocity profiles, a sine curve and slug flow profile were used. The direction of the flow was identical in all three cases. All three cases yielded identical flow fields, pressures and average friction factors.

Additionally, a slug profile with reversed sign was used at the inlet and outlet as an initial velocity profile. That is, the direction of the flow through the solution domain was reversed. The Reynolds number was identical with the previous tests. The resulting flow field was the inverse of the previous flow fields mentioned above and the average friction factor was identical. Program CRACFLO, to the extent it was tested, exhibited the ability to attain a unique solution for a unique Reynolds number and geometry ratio.

Solutions were found for $Re = 100$, $a/g = 0.5$ and 6, 12, 24 and 36 nodes cross-stream for a grid independence test. The solution for 36 nodes cross-stream did not reach full convergence; it had progressed far enough to determine the average non-dimensional pressure drop between corresponding planes but not the finest details of the flow.

The values of the average non-dimensional pressure drop between corresponding planes versus the number of nodes cross-stream for the above solutions are plotted in Figure 3-6. They show a definite trend towards an asymptotic value with increasing grid refinement, indicating a grid

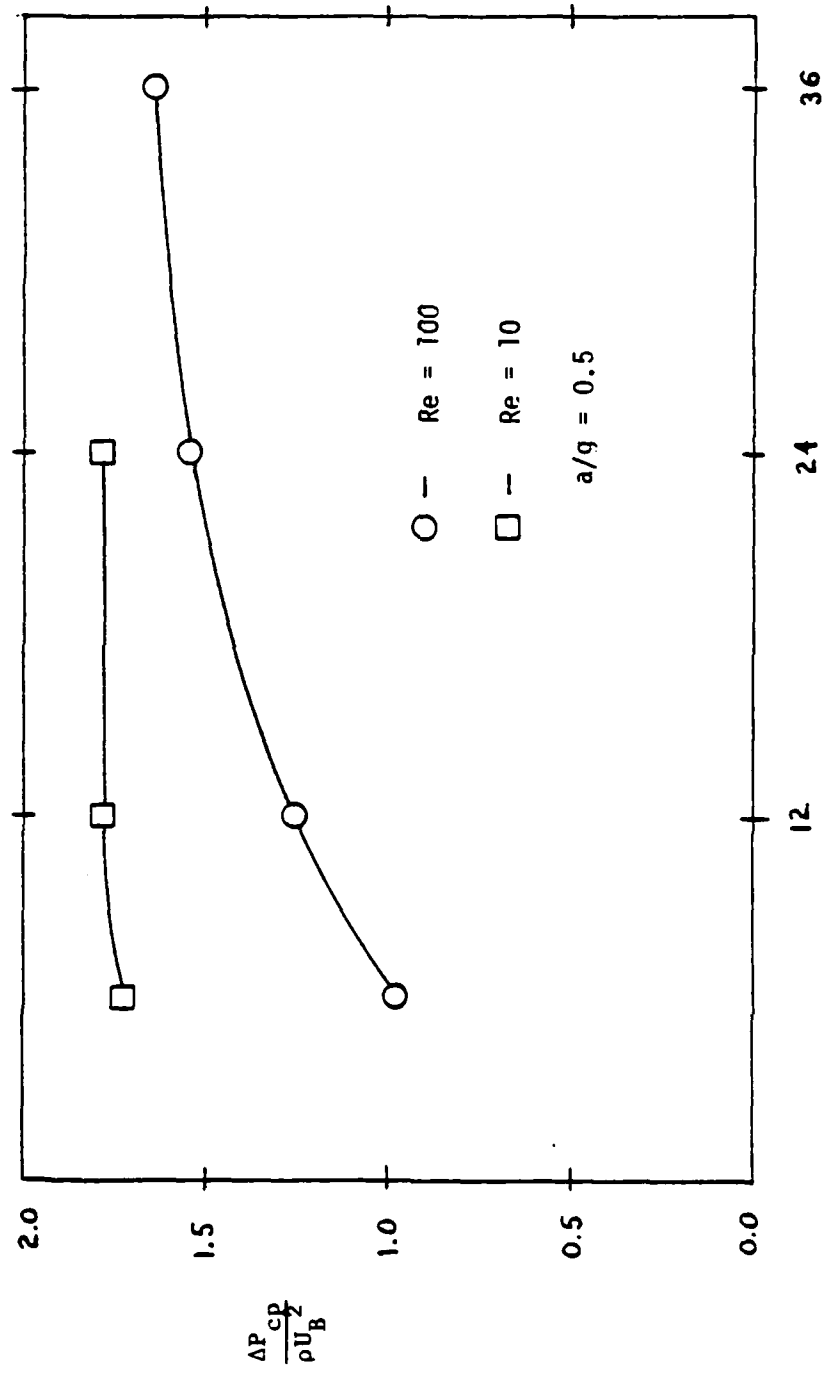

Fig. 3-6. Non-dimensional Pressure Drop Between Corresponding Planes as a Function of the Number of Nodes Cross-stream

independent solution can be obtained. This manner of plotting results of the grid independence demands more of the numerical technique in performance than other means of plotting the solution results such as against the total number of nodes in the solution domain. Hence the trend indicated in the plot is stronger evidence than may first appear.

Plotted as well in Figure 3-5 are the results for a grid independence test for Re = 10 and a/g = 0.5. Results of both grid independence tests are summarized in Table 3-1 and Table 3-2. Additionally, velocity profiles from the internal corresponding planes for the solution for Re = 100, a/g = 0.5, are plotted in Figure 3-7. Due to the staggered grid used in program TEACH, there are no values plotted in Figure 3-6 for y/g = 0.0 and y/g = 1.0. Any points apparently at these surfaces are actually for a y/g value very close to the wall. To emphasize the region near the wall, a non-uniform grid was used in all cases.

The results of the grid independence tests indicate that a grid having 12 nodes cross-stream is sufficient to produce accurate average non-dimensional pressure drops for Re $\leq$ 10. For the results presented, a grid having 24 nodes cross-stream is used for Re > 10 as a compromise between accuracy and economy.

The necessity for using more nodes cross-stream for Re > 10 seems to stem from the growth of the recirculation zones. Above Re = 10, the recirculation/separation zones grow to intersect and cross the corresponding planes. The appearance of this reversed flow at these planes injects a flow structure of finer scale than a 12 nodes cross-stream grid can adequately model. The solution is to refine the grid, in this case to a grid of 24 nodes cross-stream.

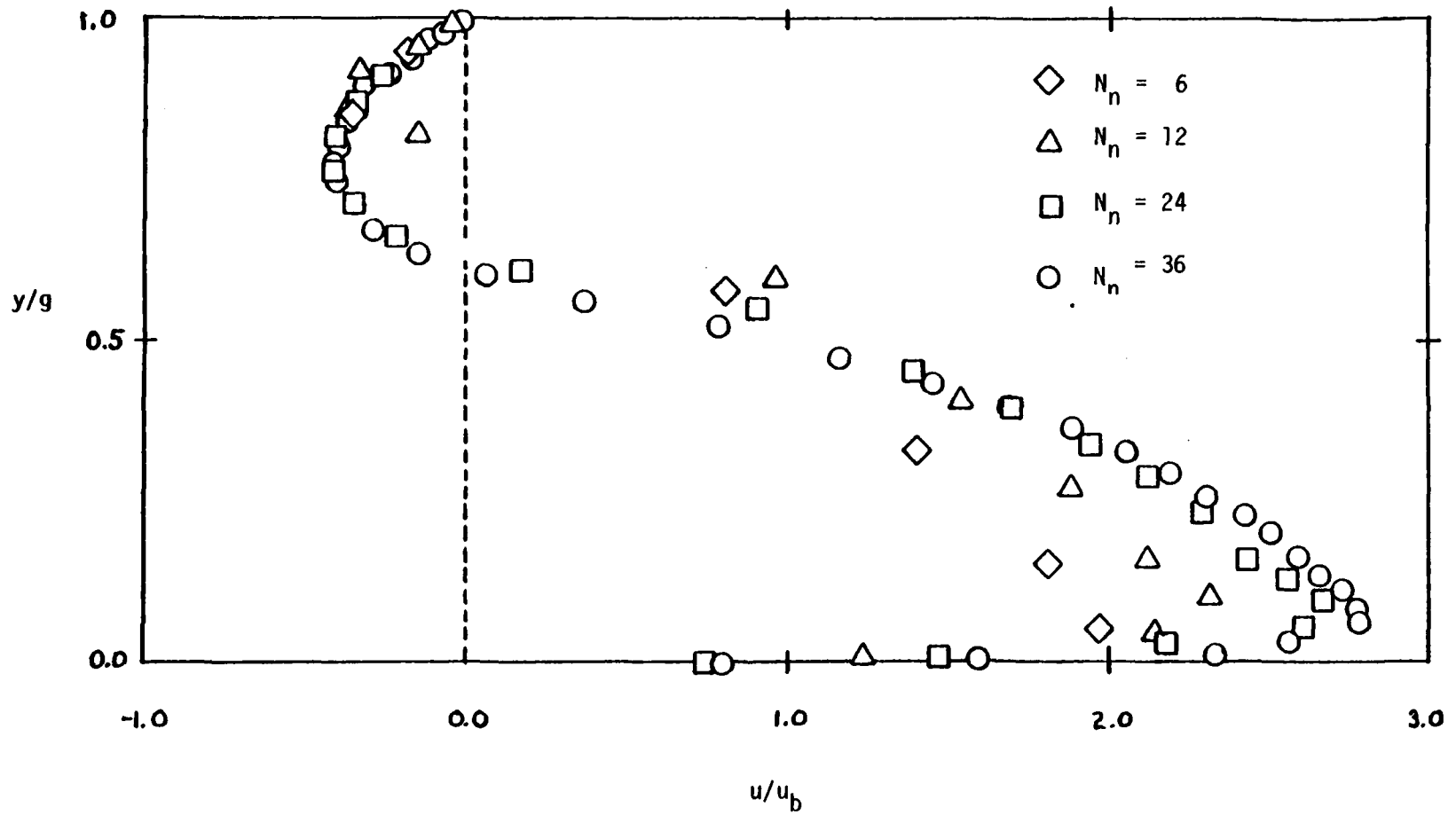

Fig. 3-7. Velocity Profiles on the Internal Corresponding Plane for Grid Independence Tests, Re = 100 and a/g = 0.5

Program RUFF

A limited test of program RUFF was performed. This test was to execute program RUFF with the rib height set to zero, i.e., as a parallel plate geometry. Analytical values of the Nusselt number and friction factor for laminar flow between parallel plates are widely available in existing literature [Kays, 1966]. These are:

$$\begin{aligned} Nu &= 8.235 \\ f &= \frac{6}{Re} \end{aligned} \tag{3-18}$$

where the Reynolds number in equation (3-18) is based on half the distance between the plates (one fourth of the hydraulic diameter) as it is in program RUFF.

Program RUFF was executed with Re = 100 and a grid of 40 x 25 nodes, of which 40 x 18 are in the fluid and the remainder are in the solid plate. The results were:

$$\begin{aligned} Nu &= 8.28 \\ f &= 0.0604 \\ Nu_w &= 8.28 \\ f_w &= 0.06 \end{aligned}$$

where the subscript w indicates a local value at the wall. Only one local value of each is tabulated; all were essentially identical.

The value of the local and average Nusselt number is 0.5% larger than the analytical value. This is considered acceptable by the author.

The friction factor, both local and average, calculated from equation (3-18) is 0.06. The local friction factors calculated by program RUFF agree very well, varying only in the fifth significant figure.

The average friction factor has a similar accuracy. The error for both local and average friction factors is 0.7% and is considered acceptable by the author.

A solution for laminar flow in a duct with repeated rib roughness was generated following this test. The results are presented in the next chapter. The grid used had non-uniform spacing with 40 nodes in the x-direction and 25 nodes in the y-direction. The region between the plate and centerline was allocated 18 nodes, in the y-direction, with 5 nodes allocated over the rib height.

3.5 Stability and Convergence

Neither program exhibited any tendency towards instability under any conditions used in the course of the author's research. The core program has its own stability requirement as described by Faas [1979; Appendix A] and was stable under all conditions.

Program CRACFLO exhibited the ability to converge towards a solution. The convergence rate, however, was lower than the author preferred. The execution time with a grid of 24 nodes cross-stream, Re = 100 and a/g = 0.5 was 188 seconds or 0.11 seconds per node on a CDC CYBER 175. The execution time with 12 nodes cross-stream, Re = 10, and a/g = 0.5 was 27.7 seconds or 0.047 seconds per node.

Program RUFF also exhibited the ability to converge uniformly to a solution, but had an even slower convergence rate. The execution time for the problem investigated was 257 seconds or 0.29 seconds per node on a CDC CYBER 175. The 24 nodes cross-stream case for CRACFLO mentioned above had a grid of 57 x 33 compared to RUFF which has 40 x 25.

3.6 The Core Program

The core program used in both program CRACFLO and RUFF is program TEACH developed by Gosman at the Imperial College, London, England. Program TEACH is documented by Gosman and Ideriah [1976] and Gosman and Pun [1973] and is described in the open literature by Khalil, Spalding and Whitelaw [1975], as well as being extensively documented by Faas [1979].

In general, TEACH solves the momentum and energy equations in terms of their primative variables for two dimensional, recirculating flows. It is necessary to have a program capable of handling recirculating flows as they often occur for rough walls. A further advantage of program TEACH is believed to be its usage of a hybrid differencing technique which uses central or upwind differencing locally according to the local flow conditions resulting in greater overall accuracy.

Modifications of program TEACH for the author's research were minimal. The only change of note was the addition of FORTRAN code to subroutine LISOLV. This code allows LISOLV to perform alternating line-by-line solutions sweeping from left to right and then top to bottom.

The change was originally made in program CRACFLO because the main flow direction of the fluid was from left to right and top to bottom, but was retained for RUFF when it was found it increased the convergence rate.

CHAPTER 4

RESULTS AND DISCUSSION

4.1 Problem CRACFLO

The Reynolds number based on the gap width g and the geometry ratio, a/g, are the controlling parameters for problem CRACFLO. Utilizing the IP method, we constructed program CRACFLO and flow solutions were produced wherein these parameters were varied. The average friction factor based on the pressure drop between corresponding planes was determined for each pair of Reynolds number and geometry ratio investigated.

Definitions

The average friction factor used in this report is defined as

$$f = -\frac{g}{\rho U_B^2}\frac{\Delta P_{cp}}{L_m} \tag{4-1}$$

where g is the gap width, L_m the mean distance between corresponding planes and ΔP_{cp} is the average pressure drop between corresponding planes defined by

$$\Delta P_{cp} = \frac{\int_{②} P_② \, d\ell}{g} - \frac{\int_{①} P_① \, d\ell}{g} \tag{4-2}$$

where the circled number subscript indicates the corresponding plane where the integration is performed and ℓ is a length variable aligned with the plane. In the program the pressure drop between the next two corresponding surfaces is also calculated to provide insight into the progress of the solution procedure.

The distance L_m is defined in Figure 4-1 as the distance along the dashed line connecting the intersecting centerplanes from A to A'. For the case illustrated, in Figure 4-1:

$$a/g = 0.5$$
$$L_m = (1.0 + a/g)g = 1.5g \qquad (4\text{-}3)$$

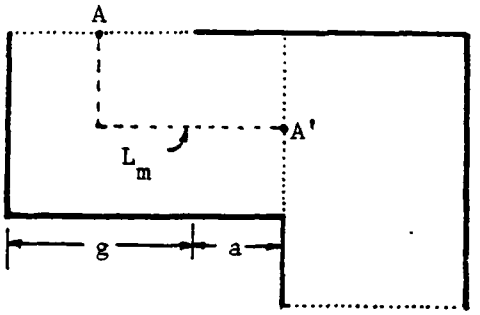

Fig. 4-1. Definition of L_m

One may note that as $a \to \infty$, the effect on the average friction factor caused by the corner regions, which correspond to the constant 1.0 in equation (4-3), becomes smaller and smaller. Hence as a approaches ∞, the average friction factor should approach that for laminar flow between parallel planes. The lower limit for a in the present version of CRACFLO is a value of 0.0.

Several geometries for a corrugated channel are presented in Figure 4-2 to give the reader an impression of the various shapes which can be calculated by the program. As a/g increases, the situation approaches a series of parallel plate ducts connected at right-angle bends.

The Reynolds number used in this report is defined by:

$$Re = \frac{\rho U_B g}{\mu} \qquad (4\text{-}4)$$

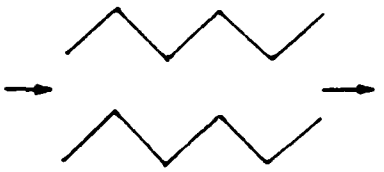

a/g = 0.0

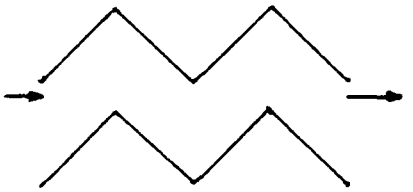

a/g = 0.5

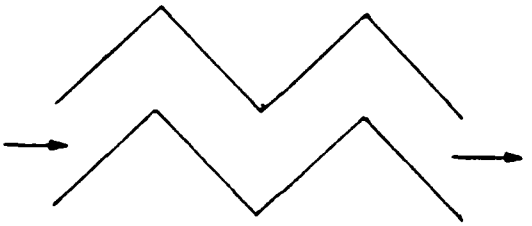

a/g = 1.0

Fig. 4-2. Sample Geometries

This definition was chosen because g was selected as the characteristic length by which all other lengths would be non-dimensionalized in problem CRACFLO.

Effect of Reynolds number on f with a/g held constant

A series of computer solutions yielding average friction factors was performed holding the geometry ratio constant while varying the Reynolds number. Two geometries were investigated; one having a geometry ratio of 0.5 and the other a geometry ratio of 0.0. The latter represents the lower limit of geometry ratios which can be calculated.

The average friction factors for these two geometries are plotted against the Reynolds number in Figures 4-3 and 4-4. Noticeable in both figures is the non-linear shape of the curves (on logarithmic coordinates) and the presence of a minimum. The typical behavior of laminar flows in ducts yields friction factor curves that are inversely proportional to the Reynolds number so they form straight lines with negative slopes on logarithmic coordinates as shown in Figure 4-4 [Knudsen and Katz, 1958].

Laminar wake flow about a circular cylinder - as well as other blunt bodies - has a drag coefficient curve, shown in Figure 4-6, similar to the curve in Figure 4-2. (However, Figure 4-6 is a semi-logarithmic plot.) Figure 4-5 also relates the behavior of the coefficient of drag to the recirculation zones or wake behind the cylinder. This observation suggests the possibility that recirculation zones in the corrugated duct may control the behavior of the average friction factor at higher Reynolds numbers.

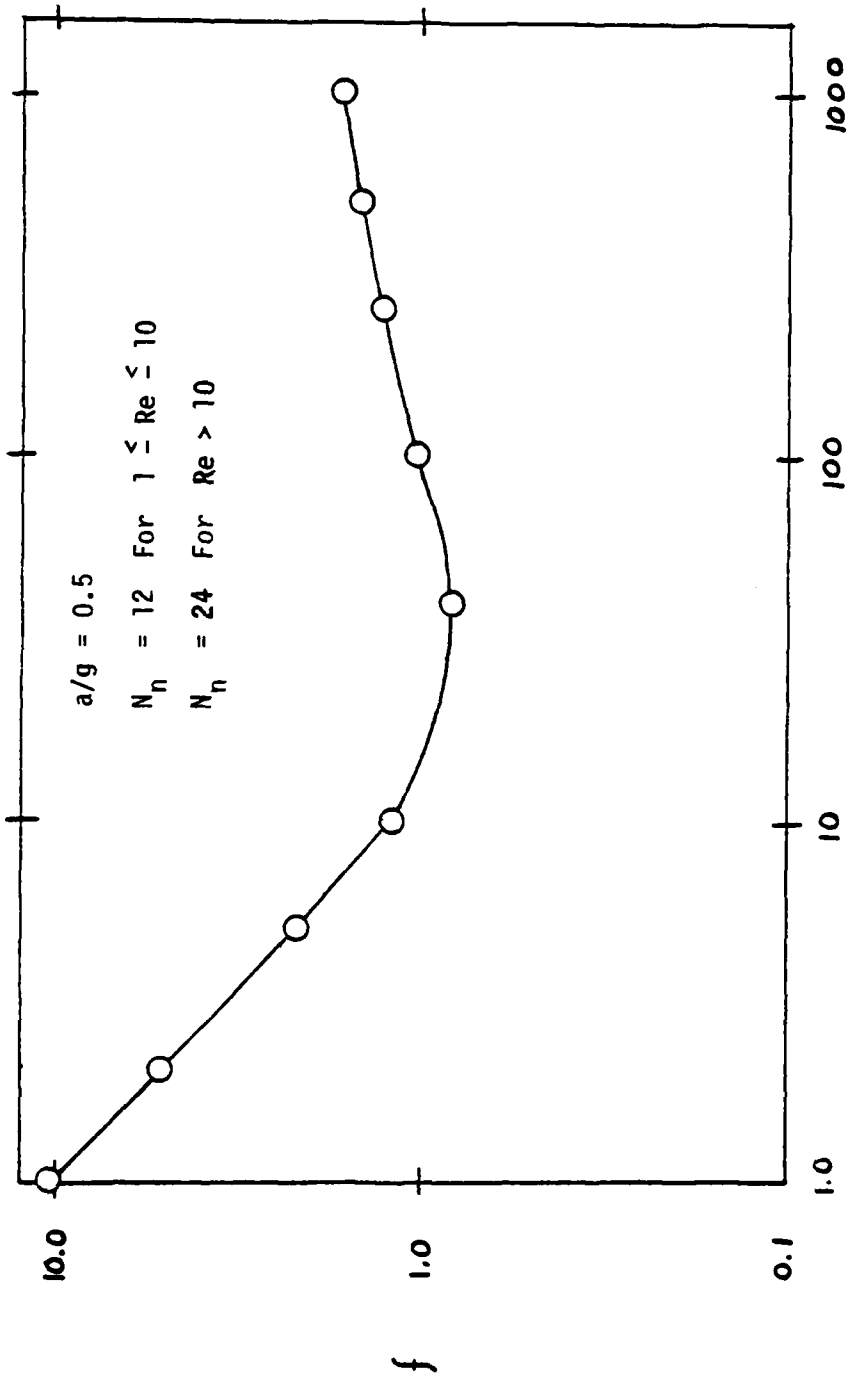

Fig. 4-3. Average Friction Factor Variation for a Geometry Ratio of 0.5

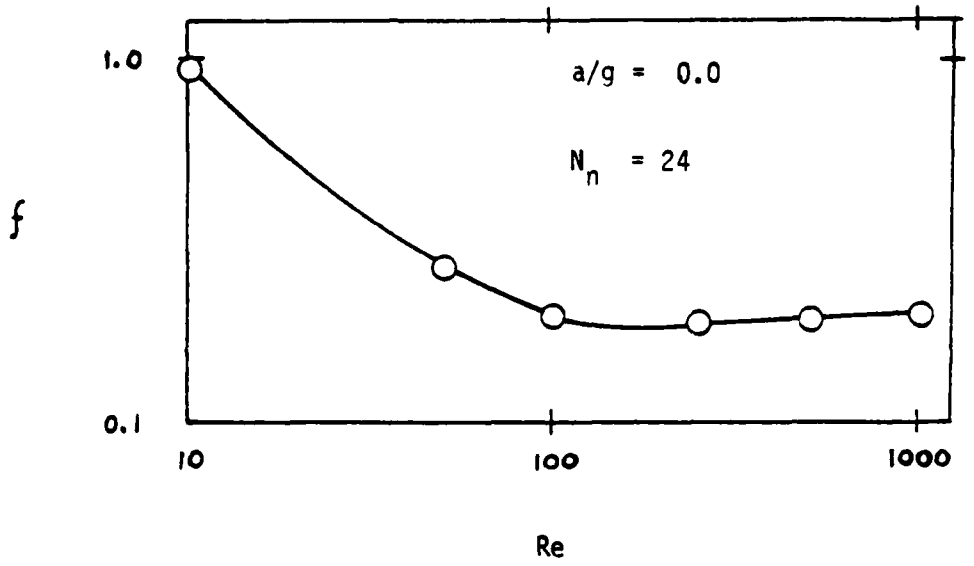

Fig. 4-4. Average Friction Factor Variation for a Geometry Ratio of 0.0

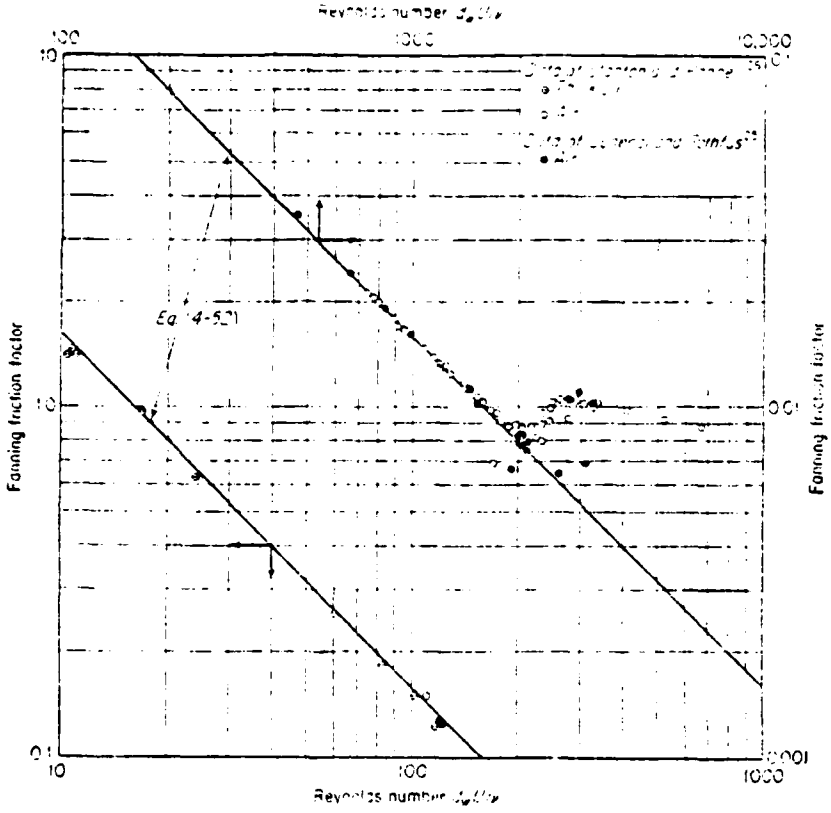

Fig. 4-5. Laminar Flow in Circular Tubes [Knudsen and Katz, 1958]

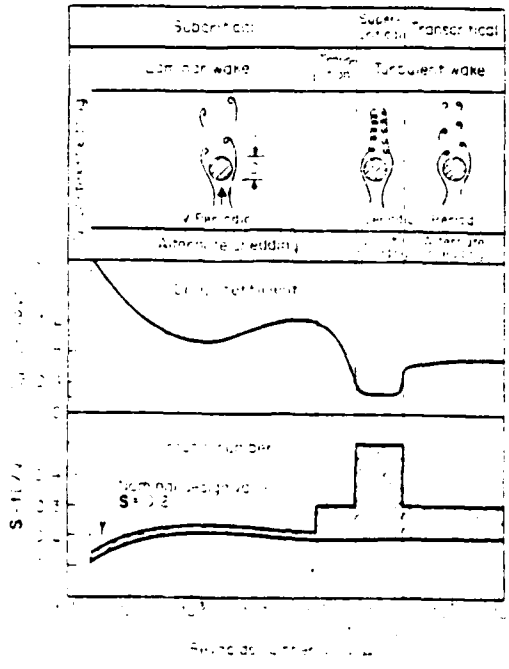

Fig. 4-6. Flow About a Circular Cylinder [Murdock, 1976]

The effect of the recirculation zones

The effect of the recirculation zones will be investigated at a constant geometry ratio, $a/g = 0.5$. A series of diagrams indicating the local flow angles in the corrugated channel aids in interpreting the size and effect of the recirculation zones. These flow angle diagrams are shown in Figures 4-2, 4-8, 4-9 and 4-10. All flow diagrams are plotted from the results of a 12-node cross-stream grid. A finer grid solution is not warranted as the gross details are of primary interest here.

The flow field in Figure 4-6 is representative of the flow for $Re \leq 10$. The recirculation zones are almost non-existant, hence the flow follows the boundaries closely and moves uniformly downstream with little or no separation or reversed flow. This flow structure is similar to Stokes' flow and it is, therefore, not surprising that the average friction factor curve is nearly linear for $Re \leq 10$ on a logarithmic plot [Schlichting, 1968].

The recirculation zones grow as the Reynolds number is increased. At $Re = 25$ the friction factor curve has diverged from its linear appearance. The recirculation zones have grown to over 1/2 g in diameter as shown in Figure 4-8. A small secondary recirculation zone, represented by a single arrow, has appeared between the major eddy and the corner. A small separation region also occurs behind the convex corner over which the fluid flows.

Figure 4-9 shows the flow field concurrent or nearly concurrent with the minimum in the average friction factor. The primary recirculation zones have grown to a diameter of approximately 3/4 g and are connected with the separated flow behind the convex corner. The secondary recirculation zones have grown as well but are still small.

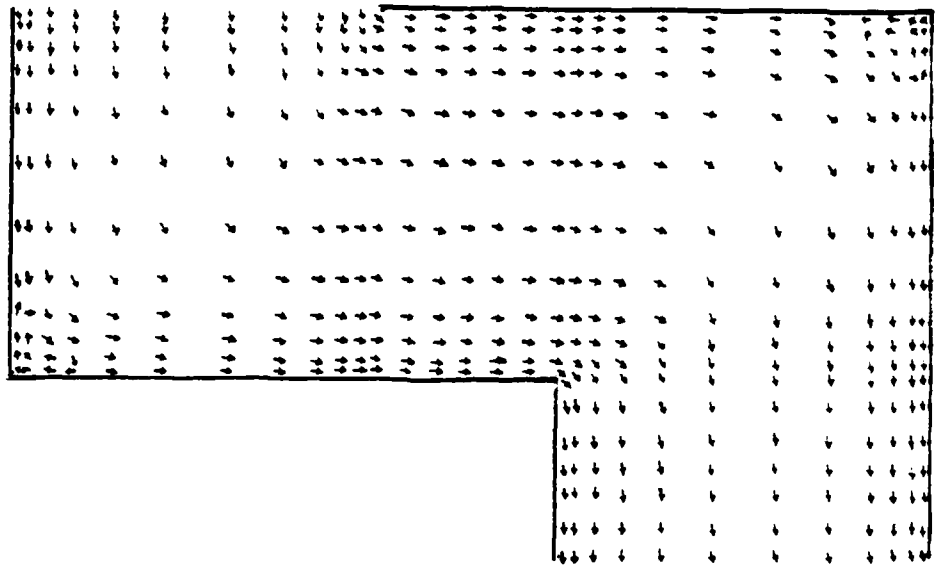

Fig. 4-7. Flow Field for Re = 10, a/g = 0.5

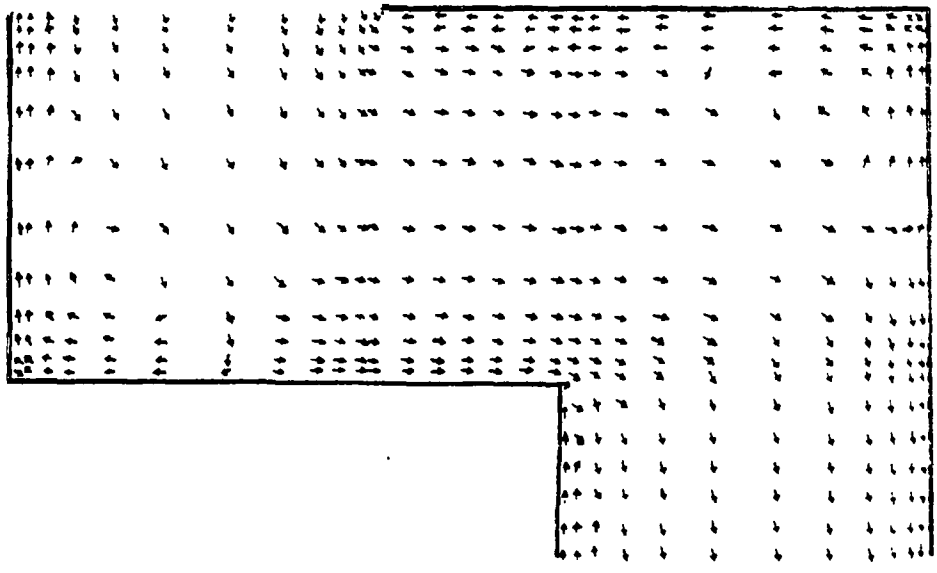

Fig. 4-8. Flow Field for Re = 25, a/g = 0.5

A flow field for a Reynolds number above that corresponding to the minimum average friction factor is shown in Figure 4-10. The primary recirculation zones have grown slightly and little change is observable in the small secondary recirculation zones.

The flow field for Re > 100 is represented by Figure 4-11. The primary recirculation zones have not changed noticeably, but the secondary recirculation zone has grown about 150 percent over its size in Figure 4-9. In both cases the main through flow streamlines appear to cross the duct relatively directly and to concentrate near the far wall after passing over a corner.

A relationship between the average friction factor and the recirculation zones may now be inferred. The recirculation zones are small or non-existent at low Reynolds numbers, consequently the average friction behaves like the friction factor for Stokes' flow. The recirculation zones grow as the Reynolds number increases and begin to affect the overall flow. This effect is characterized by the decrease in slope of the average friction factor curve.

The average friction factor reaches a minimum approximately concurrent with the stabilization of the primary recirculation zone size. Hereafter, the secondary recirculation zone grown preferentially and appears to account for the behavior of the average friction factor above Re $\gtrsim$ 100. At the higher Reynolds numbers the main throughflow becomes more concentrated and resembles a two-dimensional jet passing through a series of expansions and contractions or connected asymmetric 2-D nozzles and diffusers. The approximately constant friction factor corresponds to

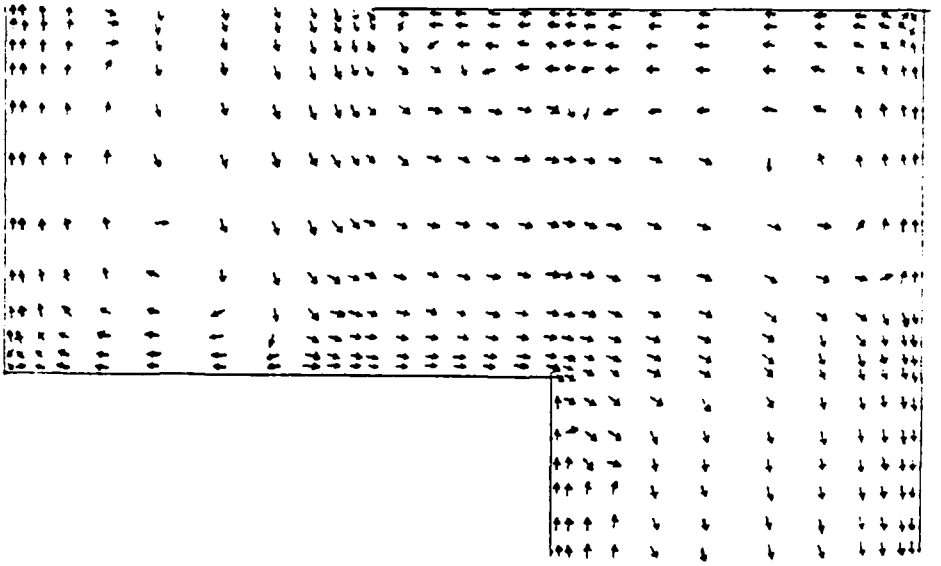

Fig. 4-9. Flow Field for Re = 50, a/g = 0.5

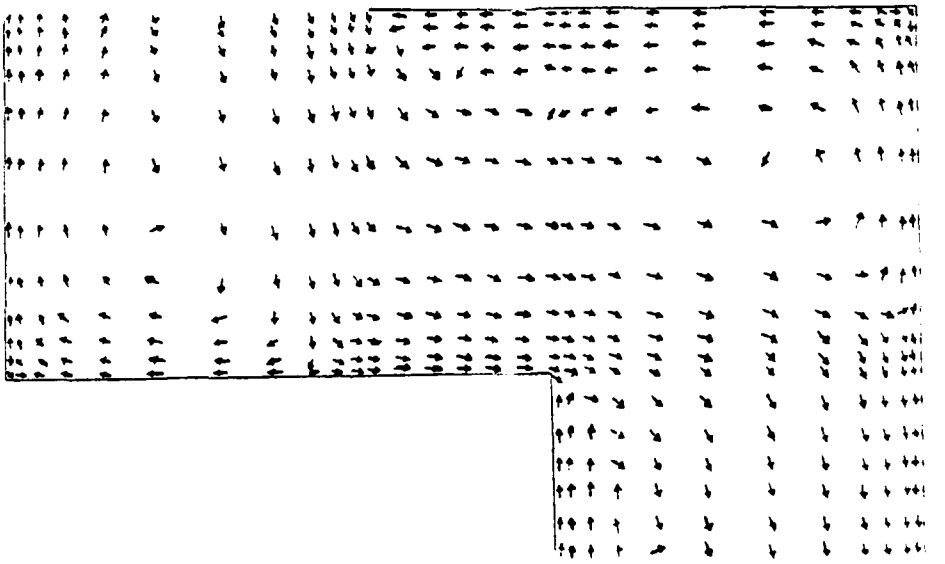

Fig. 4-10. Flow Field for Re = 100, a/g = 0.5

the loss coefficient for comparable geometries at high Reynolds numbers [Vennard and Street, 1975, sec. 9.14].

The presence of these recirculation zones may account for the differences between Figure 4-3 and the upper curve of Figure 4-12 excerpted from Kays and London [1964]. This wavy fin geometry was selected since it most closely resembles the geometry which produced Figure 4-3, i.e., a geometry ratio of 0.5. The fins of Figure 4-12 would correspond to a geometry ratio of $a/g \approx 1$ or slightly higher. The wavy fin has corner angles greater than 90 degrees whereas the corrugated channels of problem CRACFLO all have 90 degree bends. Additionally, the corners of the wavy fin are rounded but the corrugated channel corners are sharp.

These differences in geometry would tend to reduce the size of the recirculation zones by providing a more streamlined shape with less turning of the flow. The rounding of the corners would eliminate the secondary recirculation zones in the concave corners and would reduce the separation at the convex corners. Thus, it is not surprising that Figure 4-3 does not resemble the upper curve of Figure 4-12.

Curve Fits and Error Analysis

The average friction factor curves have been correlated for the range $10 \leq Re \leq 1000$. The resulting curve fit is a third-order polynomial of the form:

$$f = c_o + c_1 \log Re + c_2(\log Re)^2 + c_3(\log Re)^3 \qquad (4\text{-}5)$$

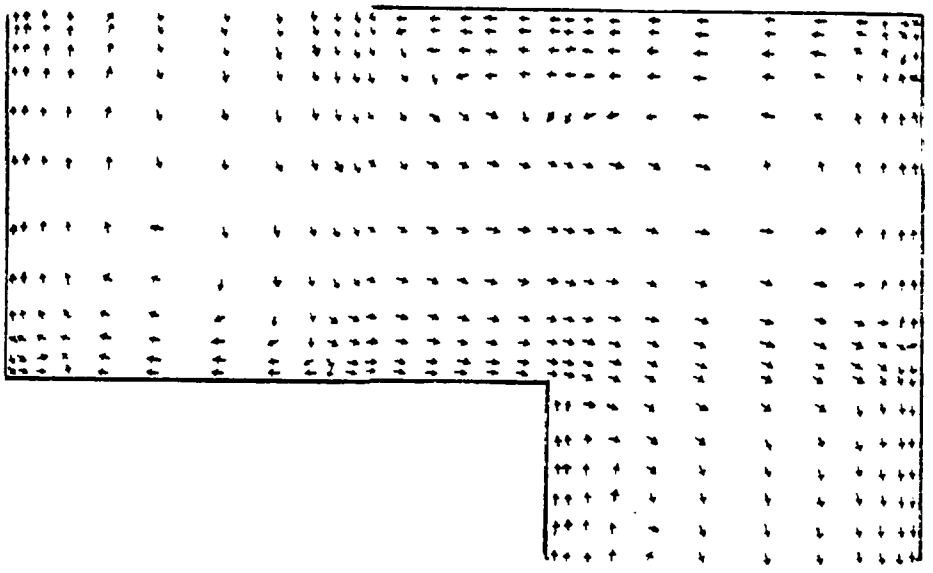

Fig. 4-11. Flow Field Diagram for Re = 250, a/g = 0.5

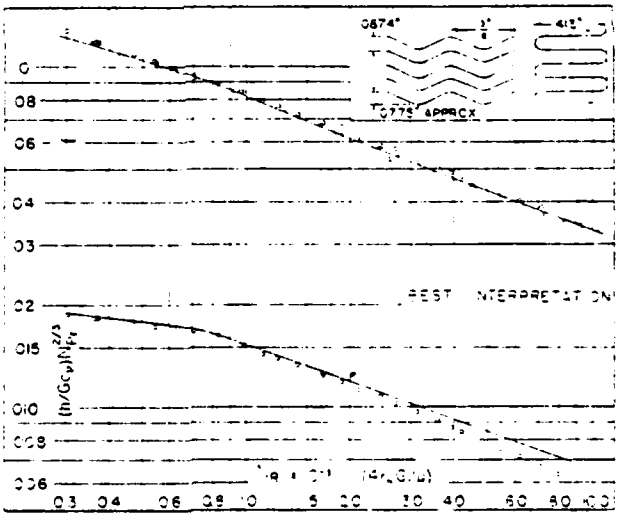

Fin pitch = 11.44 per in.

Plate spacing, b = 0.413 in.

Flow passage hydraulic diameter, $4r_h$ = 0.01060 ft

Fin metal thickness = 0.006 in., aluminum

Total heat transfer area/volume between plates, α = 351 ft²/ft³

Fin area/total area = 0.847

Note: Hydraulic diameter based on free-flow area normal to mean flow direction.

Fig. 4-12. Data for "Wavy-Fin" Duct
[Kays and London, 1964]

where the constants are:

a/g = 0.0	a/g = 0.5
$c_0 = 3.7107$	$c_0 = 5.0625$
$c_1 = -4.2743$	$c_1 = -6.633$
$c_2 = 1.7052$	$c_2 = 3.2271$
$c_3 = -0.22362$	$c_3 = -0.46658$

The accuracy of these correlations are within 7 percent of the results provided by the computer solutions. If the computer predictions are assumed to be approximately 10% low based on figure 3-5, then the overall accuracy is in the range -3.7% to -16.3%.

This accuracy was determined by the following method. The correct friction factor was defined as f_0, the computer prediction as f_1, the friction factor found by the curve fit as f_2 and the overall accuracy, ε, as

$$\varepsilon = \frac{f_0 - f_2}{f_0} \tag{4-6}$$

The friction factors may be related by

$$f_1 \tilde{=} f_0 - f_0\,(0.1) \tag{4-7}$$

$$f_2 \tilde{=} f_1 \pm f_1\,(0.07) \tag{4-8}$$

Equations (4-7) and 4-8) were combined to relate f_2 to f_0:

$$f_2 \tilde{=} f_0\,(0.09)(1.0 \pm 0.07) \tag{4-9}$$

Equation (4-9) was then substituted into equation (4-6) to estimate the overall accuracy. Unfortunately, the accuracy of the computed results is a subjective estimate and has errors of its own which presently cannot be determined.

The effect of a/g of f_1 Re held constant

The effect of varying the geometry ratio, while holding the Reynolds number constant at Re = 250, was investigated using a grid having 12 nodes cross-stream. This spacing places the numerical value of the computer results in question, but not necessarily the relative magnitudes.

The average friction factor is plotted against the geometry ratio in Figure 4-13. The average friction factor rises to a maximum at $a/g \tilde{=} 1$ and then decreases in an exponential fashion apparently approaching a constant value as a/g increases. It was previously mentioned that the average friction factor should approach the friction factor for laminar flow between parallel plates as $a \to \infty$. The trend toward a constant value in Figure 4-13 supports this hypothesis but it appears that the corner recirculation continues to dominate the pressure drop even at $a/g \lesssim 10$.

General Discussion

The results presented in this report are too incomplete to be of great utility. The correlations may be of some aid but only for the two geometries investigated. However, the potential of program CRACFLO to serve as an aid in the engineering design of corrugated fin heat exchangers in the future is not, by any means, to be overlooked.

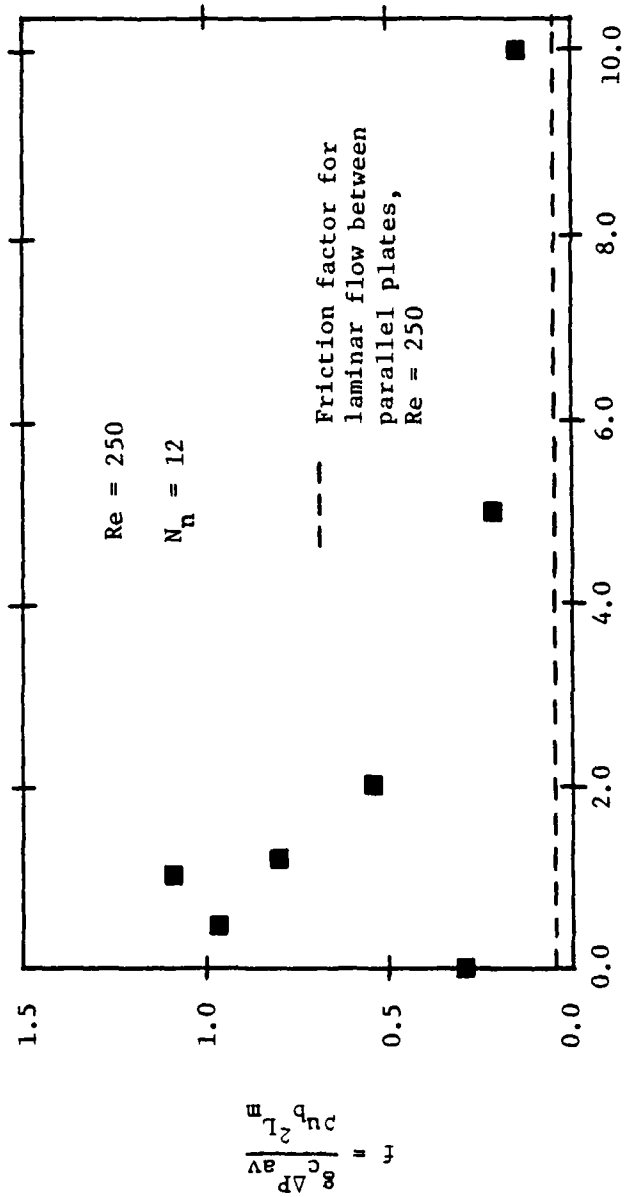

Fig. 4-13. Effect of geometry ratio, Re = 250

Perhaps the most useful observation to be made on the present results is that laminar flow in a corrugated channel may not yield the average friction factor - Reynolds number relationship

$$f \propto Re^{-1} \tag{4-10}$$

This observation has implications when one attempts to predict flow patterns in a large rock fracture and flow through a crack in a pressure vessel [Button et al. 1978]. An actual crack may have sharp or jagged walls generating recirculation zones which affect the local friction factor as in a corrugated channel. The present practice of assuming a D'Arcy relation or the presence of smooth walls to simplify the friction factor calculation is expected to be in error unless the Reynolds number is very low.

4.2 Problem RUFF

The efforts to apply the IP method to problem RUFF were initiated very close to the end of the author's research. The direct consequence was that results for only one condition - geometry, Prandtl and Reynolds numbers and thermal conductivity ratio - were produced. The discussion here will be brief as the limited results do not warrant a lengthy discourse.

Program RUFF determines local and average friction factors and Nusselt numbers in addition to the u and v velocities, pressures and temperatures. All results are non-dimensional. The local friction factors and Nusselt numbers are determined on the vertical sides of the ribs as well as on the horizontal surfaces.

Definitions

The local friction factor is defined as

$$f_w = \mu \left.\frac{\partial \vec{u}}{\partial \hat{n}}\right|_w \tag{4-11}$$

where $\hat{n}$ is a unit vector perpendicular to the surface, $\vec{u}$ is the velocity vector, and the subscript "w" indicates the values are determined at the fluid-solid interface or wall.

The local Nusselt number is defined as

$$Nu_w = \frac{\dot{q}''_w \, y_{\mathbb{C}}}{k_f \, (T_w - T_B)} \tag{4-12}$$

where $\dot{q}''_w$ is the local heat flux at the wall, T_w is the local wall temperature, $y_{\mathbb{C}}$ is the greatest distance between the plate wall and centerline (see Figure 1-5), k_f is the thermal conductivity of the fluid and the subscript "B" denotes a bulk quantity.

The average friction factor and Nusselt number are defined such that they are more useful for general design considerations. The average friction factor is defined by

$$f = - \frac{2 y_{\mathbb{C}}}{\rho U_B^2} \frac{\Delta P_{cp}}{(s + w)} \tag{4-13}$$

where ΔP_{cp} is defined in equation (4-2) replacing g with $y_{\mathbb{C}}$, s and w are the rib separation and rib width (see Figure 1-5); their sum is a rib cell length.

The average Nusselt number is defined by

$$Nu = \frac{\dot{q}''_{cell}\, y_{\mathbb{C}}}{k_f\left(T_{w_{av}} - T_{B_{av}}\right)} \tag{4-14}$$

where

$$\dot{q}''_{cell} = \frac{\int_C \dot{q}''_w \, d\ell}{(s + w)} \tag{4-15}$$

$$T_{w_{av}} = \frac{\int_C T_w \, d\ell}{(s + w + 2h)} \tag{4-16}$$

$$T_{B_{av}} = \frac{\int_o^{s+w} T_B \, dx}{(s + w)} \tag{4-17}$$

The integrals for $\dot{q}''_{cell}$ and $T_{w_{av}}$ are performed along the contour of the fluid - solid interface and ℓ is a co-ordinate for distances along the contour.

The result of using ΔP_{cp} and $\dot{q}''_{cell}$ in these average quantities is to submerge the effect of the rib into them. This allows the heat exchanger designer to perform his job without concerning himself with details, (which are available should they be of interest). One should note that for a constant heat flux applied to the outside of the repeated-rib plate, as is done in problem RUFF, that

$$\dot{q}''_{cell} = \dot{q}''_p$$

where the subscript "p" refers to the plate.

Additional information provided by program RUFF is the local flow angles and the maximum temperature in a plane perpendicular to the flow direction. The latter allows the heat exchanger designer to locate the hottest points in the heat exchanger and compensate as required.

The Reynolds number used in program RUFF is based on the wall to centerline distance, y_{ℓ}, because this is the characteristic length used to non-dimensionalize the geometry

Results

A single solution was found for the following conditions

Re = 100	$y_{\ell} = 1.0$
Pr = 0.7	s = 0.25
fluid: air	h = 0.04
plate: stainless steel	w = 0.12
$k_p/k_f = 724$	$y_p = 0.21$

The dimensions are non-dimensional and derived from the actual dimensions of a plate with repeated ribs to be used in an experimental test rig at the University of Arizona.

A heat flux, $\dot{q}''_p$, applied to the external surface of the plate was modelled as well. One should consult chapter two for a discussion on the non-dimensionalization of the energy equation and an explanation of how $\dot{q}''_p$ was imposed.

The average Nusselt number calculated was 8.48 and the average friction factor calculated was 0.07. For comparison, the Nusselt number and friction factor for laminar flow between parallel plates at the same

Reynolds number are 8.235 and 0.06, respectively, [Kays, 1966]. The calculated average Nusselt number is 2.9% greater than that for laminar flow between parallel plates. The calculated average friction factor is 16.7% greater than the friction factor for laminar flow between parallel plates which is a somewhat unexpected result. According to Schlichting [1968], the roughness element investigated should have little effect on the friction factor in laminar flow. This might be attributable to a too permissive overall convergence criterion resulting in a not fully converged solution. The convergence criterion, γ_v, was 0.005.

The local Nusselt numbers are plotted in Figure 4-14. The abscissa is the non-dimensional distance along the contour of the fluid-plate interface measured from the upstream corresponding plane. One may note the periodicity of the results and that the local Nusselt number is negative at two points indicating heat transfer to the plate. This corresponds to the point in each rib indicated by the circled dot in Figure 4-16.

The local friction factors are plotted in Figure 4-15. The abscissa is the same as was used in Figure 4-14. Here also one can note the periodicity of the results and the negative values of the friction factor. The negative values occur where recirculation is present and simply implies flow in the negative direction.

The maximum temperature at all cross-sections occurs at the external surface of the plate where $\dot{q}''_p$ is applied. This result is reasonable and predictable.

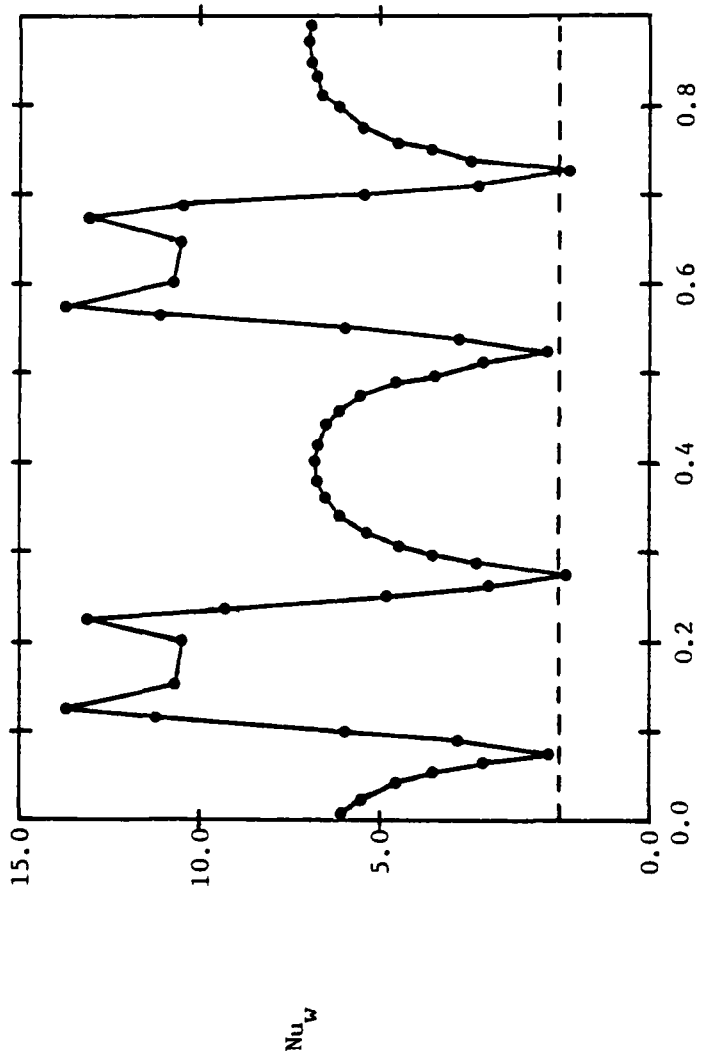

Fig. 4-14. Local Nusselt Numbers

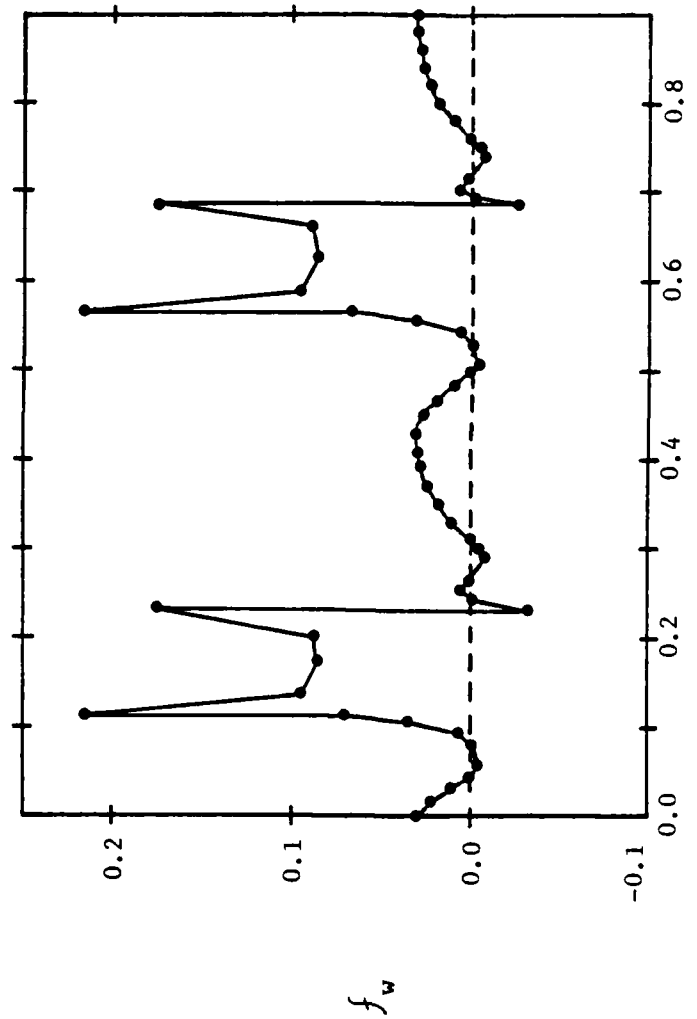

Fig. 4-15. Local Friction Factors

A plot of the local flow angles is presented in Figure 4-16 as an aid for flow visualization. Only the region above the rib where the flow is perturbed noticeably from a direction parallel with the centerline is plotted. A small recirculation zone occurs before and after the rib, the leeward recirculation zone being the larger.

The velocity profile at a boundary cross-section is plotted in Figure 4-17. The co-ordinate y_f is the distance from the fluid-plate interface measured parallel to the y-axis. The position of this cross-section relative to the rib can be reckoned from Figure 4-16 where the left or right-hand boundary is the corresponding plane location. A laminar parabolic profile is plotted as a solid line for comparison. The effect of the rib can readily be seen and its influence extends essentially to the centerline. Near the wall, the flow is still recovering from the separation caused by passing over the rib.

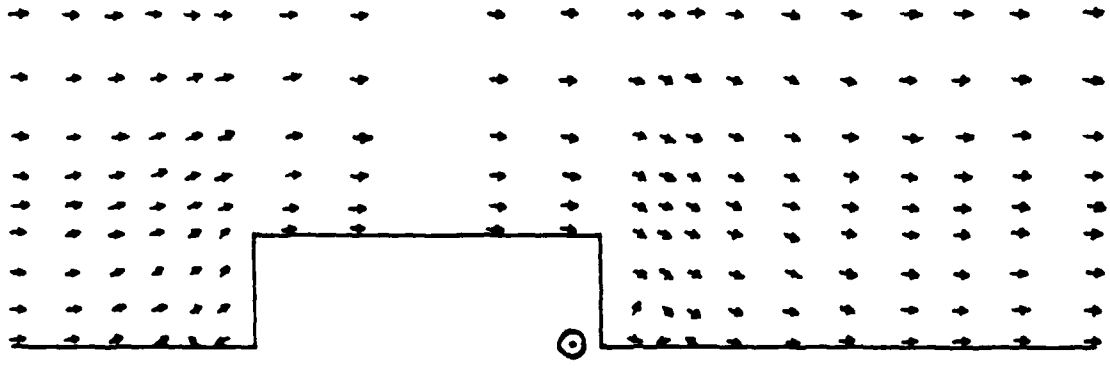

Fig. 4-16. Flow about a Rib

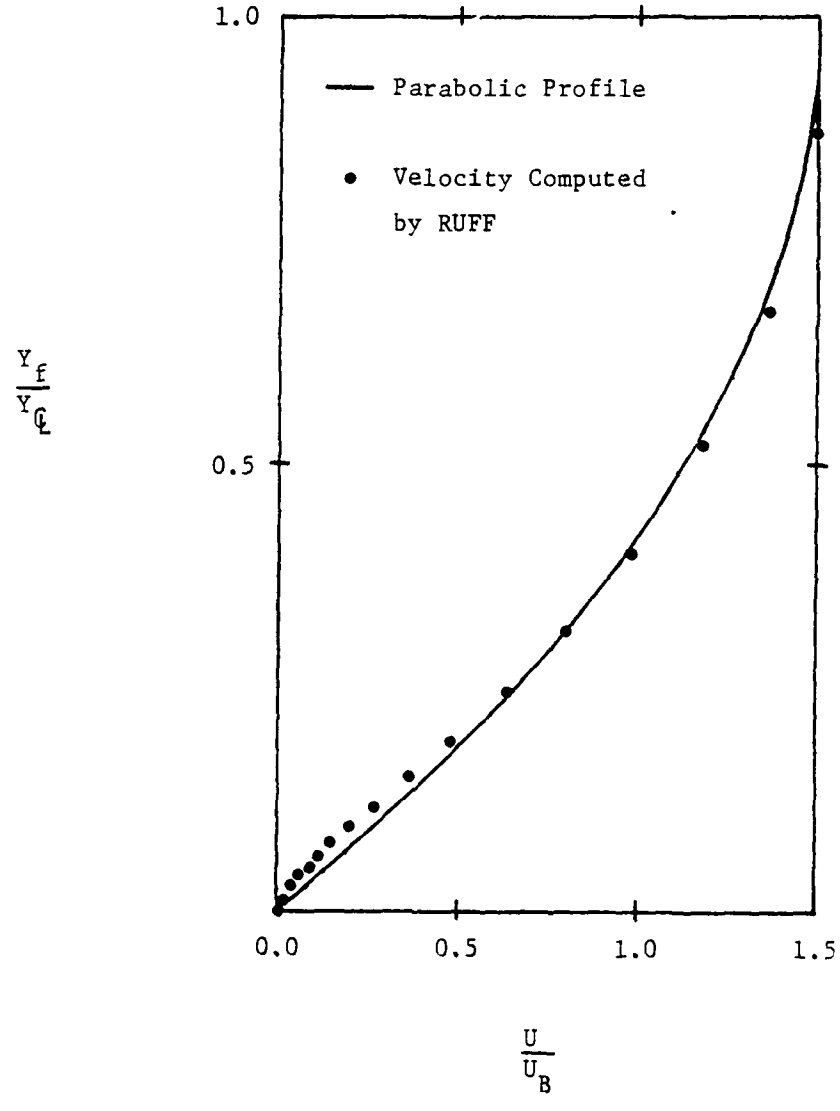

Fig. 4-17. Velocity Profile at Plane between Elements

CHAPTER 5

CONCLUSIONS AND RECOMMENDATIONS

5.1 Conclusions for Problem CRACFLO

A computer program has been successfully developed for numerically solving the fluid flow field subject to spatially periodic boundary conditions in corrugated channels with right angle bends. Preliminary results have been obtained.

The flow in this corrugated channel is seen to be more complex than might initially be anticipated; it exhibits the formation of a large primary recirculation zone and a small secondary recirculation zone as the Reynolds number increases.

As a consequence, the average friction factor passes through a minimum as the Reynolds number is varied while the geometry ratio, indicating the distance between successive bends, is held constant.

Correlations of the average friction factor as a function of Reynolds number for the two geometry ratios investigated, 0.0 and 0.5, were determined. The form of the fit is

$$f = c_0 + c_1 \log Re + c_2(\log Re)^2 + c_3(\log Re)^3$$

where the values of the constants are

a/g = 0.0	a/g = 0.5
c_0 = 3.7107	c_0 = 5.0625
c_1 = -4.2743	c_1 = -6.633
c_2 = 1.7052	c_2 = 3.2271
c_3 = -0.22362	c_3 = 0.4665

The accuracy of the curve fits are estimated as being in the range -4% to -16%.

Additionally, the effect of varying the geometry ratio while holding the Reynolds number constant on the average friction factor was investigated. It was found that the average friction factor passed through a maximum as the geometry ratio was varied and approached a constant value as the geometry ratio grew large. The latter phenomena was attributed to the lessened effect of the corner regions containing the recirculation zones on the entire flow in duct between corresponding planes.

Finally, the observed behavior of the average friction factor in corrugated channels raises doubts on the applicability of using the relation

$$f \propto Re^{-1}$$

for calculating friction factors in cracks or fractures with rough walls.

5.2 Recommendations for Problem CRACFLO

Recommendations for further work on problem CRACFLO can be grouped into three categories: a) further refinement and testing of program CRACFLO, b) production of more extensive predictions for laminar flow in corrugated channels, and c) application of program CRACFLO to new problems.

Program CRACFLO suffers from a lack of versatility. The program should be modified to have the following capabilities:

1) Ability to accurately solve for flows with geometry ratios to 25.

2) Ability to solve the thermal energy equation.

3) Ability to calculate local wall shear stresses or friction factors and local Nusselt numbers.

4) Ability to move the corresponding planes relative to the corners.

5) Ability to solve for transitional and fully turbulent flows as well as laminar flows.

6) Ability to perform solutions in less than 300 seconds on a CDC CYBER 175.

The first and fourth modifications allow for further testing of program CRACFLO, particularly to investigate the behavior of the average friction factor as the geometry ratio becomes large. The remaining modifications are to increase the utility of program CRACFLO with modification six perhaps the most important as program CRACFLO presently requires considerable execution time and is therefore expensive to use.

An important test of program CRACFLO is a laboratory experiment. This experiment is crucial for establishing the validity of predictions made by program CRACFLO. Minimum goals of the experiment would be:

a) Determine the length of the entrance region in a corrugated channel prior to the establishment of periodic flow.

b) Obtain pressure drop data to allow comparison of the average friction factors.

c) Perform flow visualization to chart the size and development of the recirculation zones.

The limited predictions presented in this report should be extended and new predictions produced. Average friction factors for a

geometry ratio of 0.0 should be determined for $1 \leq Re < 10$. New predictions of the average friction factor over the range $1 \leq Re \leq 1000$ should be produced for geometry ratios of 1.0, 1.5 and 2.0. Inspection of the geometries investigated by Kays and London [1964] indicates the geometry ratio range $0.0 \leq a/g \leq 2.0$ should cover most of the geometries that might be found in industry. The suggested new work should be regarded as a minimum goal and more predictions as desirable.

A new application would be to apply the results of program CRACFLO as input to a program predicting laminar flow in cracks. This application requires a correspondence between rock fracture geometries and the geometry ratio to be determined. This would be a difficult task, but has potentially great rewards for predicting the performance in applications such as *Hot-Dry-Rock geothermal reservoirs*.

A second new application is to modify program CRACFLO to predict the performance of corrugated absorber plates in air-cooled solar collectors. The use of solar collectors for domestic heating is a contemporary, but not a mature technology. Hence, there exists a need for investigating new methods to increase collector efficiency, and/or reduce the cost per square meter or unit of collected energy. A corrugated absorber plate may allow one or both of these goals to be attained by improving the performance by heat transfer augmentation [McEligot and Bankston, 1979].

5.3 Conclusions for Problem RUFF

A program has been successfully developed for numerically solving for laminar flow and heat transfer subject to periodic conditions in parallel plate ducts with repeated rib roughness and a constant imposed heat flux applied to the external plate surface.

A single case was investigated. An average Nusselt number 3% greater and an average friction factor 16.7% greater than those for laminar flow between parallel plates were found. The average friction factor result is believed to reflect a not fully converged solution.

Local Nusselt numbers and friction factors were determined as well. The results indicate that heat is transferred to the plate at the base of the leeward side of the rib and that recirculation zones occur before and after the rib.

The leeward recirculation zone is found to be larger than the windward recirculation zone. The rib affects the velocity profile at a plane approximately midway between it and the following rib, from the wall to essentially the centerline.

5.4 Recommendations for Problem RUFF

Recommendations for further work on problem RUFF can be grouped into two categories: a) further refinement and testing of program RUFF, and b) application of program RUFF to problems.

Program RUFF was brought to an operational state by the author in the course of his research, but many tests have yet to be performed. The effect on the calculated flow field of the boundary plane location relative to the rib must be investigated. Grid independence tests must be performed and the effect of alternate initial flow fields investigated. The overall convergence criterion must be decreased until the average friction factor becomes insensitive to it.

A major goal is to reduce the computational time presently required by program RUFF. The cyclic tri-diagonal matrix method mentioned in Chapter 3 and described by Faas [1979; Appendix D] may provide a solu-

tion to this problem. Another major goal is to modify RUFF to handle transitional and turbulent flows as these are of greater interest.

The existing literature should be surveyed to find experimental data to aid in verifying program RUFF and aiding in its development. Conducting laboratory experiments may be necessary as well.

Program RUFF should eventually be used in the design and optimization of heat transfer surface using repeated rib roughness to enhance heat transfer. The current grid scheme of program RUFF restricts application so only small roughness elements can be treated; modifications should be made to allow roughness elements on the order of half the plate spacing to be investigated. Other geometries, such as staggered ribs and ribs on a single wall of the duct are extensions of program RUFF that should be easily realized and of interest. Program RUFF may have applications in predicting flow in cracks as well as Program CRACFLO.

Table 4-1. Friction factor as a function of Reynolds number for $a/g = 0.0$ and $N_n = 24$

Reynolds Number, Re	Non-Dimensional Pressure, $\frac{\Delta P_{cp}}{\rho U_b^2}$	Friction Factor
10.0	0.9181	0.9181
50.0	0.2572	0.2572
100.0	0.194	0.194
250.0	0.183	0.183
500.0	0.186	0.186
1000.0	0.197	0.197

Table 4-2. Friction factor as a function of Reynolds number for $a/g = 0.5$ and $N_n = 24$

Reynolds Number, Re	Non-Dimensional Pressure, $\frac{\Delta P_{cp}}{\rho U_b^2}$	Friction Factor
10.0	1.786	1.19
50.0	1.230	0.82
100.0	1.540	1.03
250.0	1.921	1.28
500.0	2.181	1.45
1000.0	2.41	1.61

Table 4-3. Friction factor as a function of Reynolds number for $a/g = 0.5$ and $N_n = 12$

Reynolds Number, Re	Non-Dimensional Pressure Drop, $\frac{\Delta P_{cp}}{\rho U_b^2}$	Friction Factor
1.0	15.37	10.3
2.0	7.728	5.15
5.0	3.203	2.14
10.0	1.783	1.19
25.0	1.135	0.757
50.0	1.095	0.730
100.0	1.255	0.837
250.0	1.454	0.969
500.0	1.656	1.10
1000.0	1.861	1.24

Table 4-4. Friction factor as a function of geometry ratio, a/g, for Re = 250 and N_n = 12

Geometry Ratio, a/g	Non-Dimensional Pressure Drop, $\frac{\Delta P_{co}}{\rho U_b^2}$	Friction Factor
0.0	0.2857	0.286
0.5	1.454	0.969
1.0	2.165	1.08
1.5	1.968	0.787
2.0	1.608	0.536
5.0	1.258	0.210
10.0	1.601	0.146

REFERENCES

Beloborodov, V. G. and B. P. Volgin, 1971. "Heat Transfer and Pressure Drop in Heat Transfer Equipment with Slot Channels of Varying Cross Section," International Chemical Engineering, Vol. II, No. 2, pp. 229-233.

Bergles, A. E., 1978. "Enhancement of Heat Transfer," Proc. 6th Intl. Heat Transfer Conf., Vol. 6, pp. 89-108.

Button, B. L., A. F. Grogan, T. C. Chivers, and P. T. Manning, 1978. "Gas Flow Through Cracks," Journal of Fluids Engineering, Vol. 100, No. 4, pp. 453-458.

Cebeci, T. and P. Bradshaw, 1977. Momentum Transfer in Boundary Layers, Washington; Hemisphere.

Faas, S. E., 1979. "Numerical prediction of flows in two-dimensional ducts with repeating surface geometries," M.S.E. report, Aero. Mech. Engr., University of Arizona.

Goldstein, L. and E. M. Sparrow, 1976. "Experiments on the Transfer Characteristics of a Corrugated Fin and Tube Heat Exchanger Configuration," Journal of Heat Transfer, Vol. 98, No. 2, pp. 26-34.

Goldstein, L. and E. M. Sparrow, 1977. "Heat/Mass Transfer Characteristics for Flow in a Corrugated Wall Channel," Journal of Heat Transfer, Vol. 99, No. 5, pp. 187-195.

Gosman, A. D. and F. J. K, Ideriah, 1976. "TEACH-T: A General Computer Program for Two-Dimensional, Turbulent, Recirculating Flows," manuscript of technical report, Mechanical Engineering, Imperial College of Science and Technology, London, England.

Gosman, A. D. and W. M. Pun, 1973. "Calculation of Recirculating Flows," Technical Report HTS/74/2, Mechanical Engineering, Imperial College of Science and Technology, London, England.

Jennings, Alan, 1977. Matrix Computation for Engineers and Scientists, John Wiley and Sons, Inc., New York.

Kays, W. M., 1966. Convective Heat and Mass Transfer, McGraw-Hill, New York.

Kays, W. M. and A. L. London, 1964. Compact Heat Exchangers, McGraw-Hill, New York.

Khalil, E. E., D. B. Spalding and J. H. Whitelaw, 1975. "The calculation of local flow properties in two-dimensional furnaces," Int. J. Heat Mass Transfer, 18, pp. 775-791.

Knudsen, J. G. and D. L. Katz, 1958. Fluid Dynamics and Heat Transfer, McGraw-Hill, New York.

Lewis, M. J., 1975. "An Elementary Analysis for Predicting the Momentum- and Heat-Transfer Characteristics of a Hydraulically Rough Surfact," Journal of Heat Transfer, Vol. 97, No. 2, pp. 249-254.

Lewis, M. J., 1975. "Optimizing the Thermohydraulic Performance of Rough Surfaces," International Journal of Heat and Mass Transfer, Vol. 18, No. 11, pp. 1243-1248.

McEligot, D. M. and C. A. Bankston, 1979. "Forced convection in solar collectors," Proc., Int. Congr., ISES, Atlanta.

McFarland, R. D., 1975. "Geothermal Reservoir Models - Crack Plane Model," LA-5947-MS, Los Alamos Scientific Laboratory Report.

McFarland, R. D. and H. D. Murphy, 1976. "Extracting Energy from Hydraulically Fractured Geothermal Reservoirs," paper submitted to the 11th Intersociety Energy Conversion Engineering Conference, State Line, Nev., Sept. 12-17, 1976.

Murdock, J. W., 1976. Fluid Mechanics and its Applications, Houghton-Mifflin.

Nemat-Nasser, S. and M. Ohtsubo, 1978. "Fluid Flow and Heat Transfer Through Hydraulically Induced Fractures in Hot, Dry Rock Masses," Journal of Pressure Vessel Technology, Vol. 100, No. 3, pp. 277-284.

Patankar, S. V., C. H. Liu, and E. M. Sparrow. "Fully Developed Flow and Heat Transfer in Ducts Having Streamwise-Periodic Variations of Cross-Sectional Area," Journal of Heat Transfer, Vol. 99, pp. 180-186.

Schlichting, M., 1968. Boundary-Layer Theory, McGraw-Hill, New York.

Short, B. E., 1977. "Numerical Prediction of Heated Flow Between Repeated Rib Rough Surfaces," M.S.E. report, Aero. Mech. Engr., University of Arizona.

Vennard, J. K., and R. L. Street, 1975. Elementary Fluid Mechanics, 5th Ed., John Wiley and Sons, New York.

Webb, R. L., 1978. "Toward a Common Understanding of the Performance and Selection of Roughness for Forced Convection," Paper 78-WA/HT-61, ASME Heat Transfer Division.

DISTRIBUTION LIST

HEAT TRANSFER

	One copy except as noted
Mr. M. Keith Ellingsworth Power Program Office of Naval Research 800 N. Quincy Street Arlington, VA 22203	5
Defense Documentation Center Building 5, Cameron Station Alexandria, VA 22314	12
Technical Information Division Naval Research Laboratory 4555 Overlook Avenue SW Washington, DC 20375	6
Professor Paul Marto Department of Mechanical Engineering US Naval Post Graduate School Monterey, CA 93940	
Professor Bruce Rankin Naval Systems Engineering US Naval Academy Annapolis, MD 21402	
Office of Naval Research Eastern/ Central Regional Office Bldg 114, Section D 666 Summer Street Boston, Massachusetts 02210	
Office of Naval Research Branch Office 536 South Clark Street Chicago, Ill. 60605	
Office of Naval Research Western Regional Office 1030 East Green Street Pasadena, CA 91106	
Mr. Charles Miller, Code 05R13 Crystal Plaza #6 Naval Sea Systems Command Washington DC 20362	

Enclosure (2)

Steam Generators Branch, Code 5222
National Center #4
Naval Sea Systems Command
Washington, DC 20362

Heat Exchanger Branch, Code 5223
National Center #3
Naval Sea Systems Command
Washington, DC 20362

Mr. Ed Ruggiero, NAVSEA 08
National Center #2
Washington, DC 20362

Dr. Earl Quandt Jr., Code 272
David Taylor Ship R&D Center
Annapolis, MD 21402

Mr. Wayne Adamson, Code 2722
David Taylor Ship R&D Center
Annapolis, MD 21402

Dr. Win Aung
Heat Transfer Program
National Science Foundation
Washington, DC 20550

Mr. Michael Perlsweig
Department of Energy
Mail Station E-178
Washington, DC 20545

Dr. W.H. Thielbahr
Chief, Energy Conservation Branch
Dept. of Energy, Idaho Operations Office
550 Second Street
Idaho Falls, Idaho 83401

Professor Ephriam M. Sparrow
Department of Mechanical Engineering
University of Minnesota
Minneapolis, Minnesota 55455

Professor J.A.C. Humphrey
Department of Mechanical Engineering
University of California, Berkeley
Berkeley, California 94720

Professor Brian Launder
Thermodynamics and Fluid Mechanics Division
University of Manchester
Institute of Science & Technology
P088 Sackville Street
Manchester M601QD England

Professor Shi-Chune Yao
Department of Mechanical Engineering
Carnegie-Mellon University
Pittsburgh, PA 15213

AD-A094 249 ARIZONA UNIV TUCSON ENGINEERING EXPERIMENT STATION F/G 20/13
CONVECTIVE HEAT TRANSFER FOR SHIP PROPULSION.(U)
JAN 80 S E FAAS, D M MCELIGOT N00014-75-C-0694
UNCLASSIFIED 1248-7 NL

2 to 2

END
DATE FILMED
2-81
DTIC

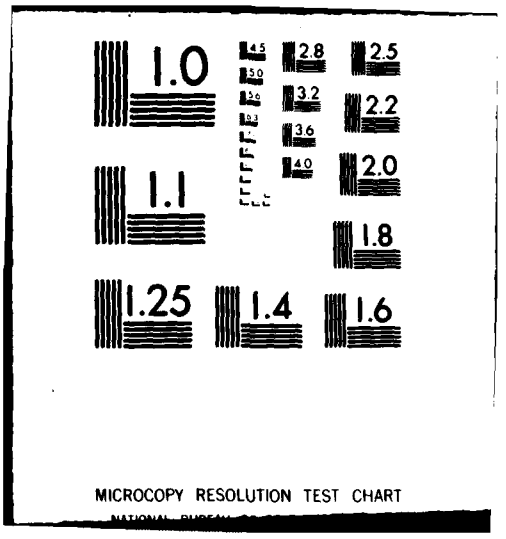
1.0
1.1
1.25
1.4
1.6
1.8
2.0
2.2
2.5
2.8
3.2
3.6
4.0
4.5
5.0
5.6
6.3
MICROCOPY RESOLUTION TEST CHART

Professor Charles B. Watkins
Chairman, Mechanical Engineering Department
Howard University
Washington, DC 20059

Professor Adrian Bejan
Department of Mechanical Engineering
University of Colorado
Boulder, Colorado 80309

Professor Donald M. McEligot
Department of Aerospace and Mechanical Engineering
Engineering Experiment Station
University of Arizona 85721

Professor Paul A. Libby
Department of Applied Mechanics and Engineering Sciences
University of California San Diego
Post Office Box 109
La Jolla, CA 92037

Professor C. Forbes Dewey Jr.
Fluid Mechanics Laboratory
Massachusetts Institute of Technology
Cambridge, Massachusetts 02139

Professor William G. Characklis
Dept. of Civil Engineering and Engineering Mechanics
Montana State University
Bozeman, Montana 59717

Professor Ralph Webb
Department of Mechanical Engineering
Pennsylvania State University
208 Mechanical Engineering Bldg.
University Park, PA 16802

Professor Warren Rohsenow
Mechanical Engineering Department
Massachusetts Institute of Technology
77 Massachusetts Avenue
Cambridge, Massachusetts 02139

Professor A. Louis London
Mechanical Engineering Department
Bldg. 500, Room 5018
Stanford University
Stanford, CA 94305

Professor James G. Knudsen
Associate Dean, School of Engineering
Oregon State University
219 Covell Hall
Corvallis, Oregon 97331

1

Professor Arthur E. Bergles
Mechanical Engineering Department
Iowa State University
Ames, Iowa 50011

Professor Kenneth J. Bell
School of Chemical Engineering
Oklahoma State University
Stillwater, Oklahoma 74074

Dr. James Lorenz
Component Technology Division
Argonne National Laboratory
9700 South Cass Avenue
Argonne, Illinois 60439

Dr. David M. Eissenberg
Oak Ridge National Laboratory
P.O. Box Y, Bldg. 9204-1, MS-0
Oak Ridge, Tennessee 37830

Dr. Jerry Taborek
Technical Director
Heat Transfer Research Institute
1000 South Fremont Avenue
Alhambra, CA 91802

Dr. Simion Kuo
Chief, Energy Systems
Energy Research Laboratory
United Technology Research Center
East Hartford, Connecticut 06108

Mr. Jack Yampolsky
General Atomic Company
P.O. Box 81608
San Diego, CA 92138

Mr. Ted Carnavos
Noranda Metal Industries, Inc.
Prospect Drive
Newtown, Connecticut 06470

Dr. Ramesh K. Shah
Harrison Radiator Division
General Motors Corporation
Lockport, New York 14094

Dr. Ravi K. Sakhuja
Manager, Advanced Programs
Thermo Electron Corporation
101 First Avenue
Waltham, Massachusetts 02154

Mr. Robert W. Perkins
Turbotec Products, Inc.
533 Downey Drive
New Britain, Connecticut 06051

Dr. Keith E. Starner
York Division, Borg-Warner Corp.
P.O. Box 1592
York, PA 17405

Mr. Peter Wishart
C-E Power Systems
Combustion Engineering, Inc.
Windsor, Connecticut 06095

Mr. Henry W. Braum
Manager, Condenser Engineering Department
Delaval
Front Street
Florence, New Jersey 08518

Dr. Thomas Rabas
Steam Turbine-Generator Technical Operations Division
Westinghouse Electric Corporation
Lester Branch
P.O. Box 9175 N2
Philadelphia, PA 19113